This is a non-peer-reviewed preprint submitted to EarthArXiv.

The original version of this manuscript has been submitted for publication in Nature Geoscience on 22nd Mar 2024. Please note the manuscript has yet to be formally accepted for publication. Subsequent versions of this manuscript may have slightly different content. If accepted, the final version of this manuscript will be available via the 'Peer-reviewed Publication DOI' link on the right-hand side of this webpage. Please feel free to contact any of the authors; we welcome feedback.

Large-scale rotational extension triggered basin formation in interior East Antarctica

Egidio Armadillo[1]*, Daniele Rizzello[1]†, Pietro Balbi[1]‡, Alessandro Ghirotto[1]§, Davide Scafidi[2], Guy Paxman[3], Andrea Zunino[4], Fausto Ferraccioli[5,6], Laura Crispini[2], Andreas Läufer[7], Frank Lisker[8], Antonia Ruppel[7], Danilo Morelli[2] and Martin Siegert[9]

[1]Applied Geophysics Laboratory, DISTAV, University of Genoa, Genoa, Italy

[2]DISTAV, University of Genoa, Genoa, Italy

[3]Department of Geography, Durham University, Durham, United Kingdom

[4]Institute of Geophysics, Swiss Federal Institute of Technology (ETH), Zürich, Switzerland

[5]National Institute of Oceanography and Applied Geophysics (OGS), Trieste, Italy

[6]British Antarctic Survey (BAS), NERC, Cambridge, United Kingdom

[7]Federal Institute for Geosciences and Natural Resources (BGR), Hannover, Germany

[8]Department of Geosciences, University of Bremen, Bremen, Germany

[9]University of Exeter, Exeter, United Kingdom

*Corresponding author. Email: egidio.armadillo@unige.it

†Current address: Tellus-Explora S.a.s., Genoa, Italy

‡Current address: Italferr S.p.a., Genoa, Italy

§Current address: Institute of Geophysics, Swiss Federal Institute of Technology (ETH), Zürich, Switzerland

Declarations:

This preprint paper was submitted on 22nd Mar 2024 to "Nature Geoscience" for peer review.

Abstract

Recent sub-ice topography investigations have imaged with greatly improved detail a set of enigmatic low-elevation V-shaped basins hidden beneath a very large sector of the East Antarctic Ice Sheet. Here we show that these basins form a semi-continental sized fan shaped physiographic unit which radiates from a pin point near the South Pole and name it the East Antarctic Fan-shaped Basin Province. By jointly interpreting sub-ice topography and geophysical data, we demonstrate that the fan-like landscape originated from a distributed intraplate rotational extension before Gondwana breakup which had three continental-scale consequences. i) Laterally, to the west, it caused compression and the consequent uplift of the Gamburtsev Mountains. ii) To the east, the northernmost Transantarctic Mountains segment was rotated clockwise of ~20° overriding the West Antarctic Rift System's hot lithosphere, causing segmentation of the mountain chain into three blocks and their differential uplift due to thermal buoyancy. iii) To the North, the transcurrent edge of the fan formed the lithospheric weakness that controlled the break-up of Gondwana by driving the propagation of Antarctica/Australia separation and shaping the resulting semi-circular passive continental margins. These processes have substantially influenced the present-day East Antarctica sub-ice landscape and the evolution of the overlying ice-sheet.

MAIN

Observation and measurement of Antarctic bedrock is hindered by the Antarctic Ice Sheet, which covers more than 99% of the continent. Recently, international compilations of radio-echo sounding investigations[1,2] have resolved large-scale subglacial topographic features at increasingly high levels of detail revealing a wide and low-elevation sector of East Antarctica extending from Prydz Bay (70° E) to the Transantarctic Mountains (160° E) and from the coastlines to 85° S (Fig. 1). In this region, most of the large subglacial basins and trenches, containing sediments of variable estimated thickness[3-5], present an enigmatic spatial V-shape and are intriguingly aligned along the north-south direction, converging approximately towards the South Pole (Extended Data Fig. 1). Moreover, the 2000 km long Antarctic coastline and continent-ocean boundary margin, delimiting the sector to the north, has a distinct semicircular arc geometry. Consequently, at a semi-continental scale, the topography resembles a 'handheld fan', converging to a pin point located close to the South Pole (Fig. 1). We propose the whole region to be a single physiographic unit and name it the

East Antarctic Fan-shaped Basin Province (EAFBP). We reveal how the EAFBP formed within the context of Gondwana breakup. As the V-shaped basins underlie almost half of the East Antarctic Ice Sheet, they will influence heavily both ice-flow and landscape evolution[3-6], making them important to Antarctic glacial and hydrological processes.

Sub-ice topographical observations

By detailed analysis of the subglacial morphological features (Methods), we identified 30 basins comprising the EAFBP (Extended Data Tab. 1), all of which are elongated along the north-south direction and many exhibit an approximately V-shape (Fig. 1). Together, the basins form a fan with an axis of symmetry passing through the Belgica Subglacial Highlands, approximately aligned along the meridian 130°E, here named the Belgica bisector. This bisector divides the EAFBP into the sinistral (SX) sector to the west and the dextral (DX) sector to the east.

To quantitatively define the geometry of the fan and estimate its pivot point location, we fitted the detected main longitudinal edges of the basins to great circles on the globe (Extended Data Fig. 2 and Methods), which in planar view are represented by straight lines converging to the pivot point EP located at 86.4°S, 129.9°E (Fig. 1).

The EAFBP consists of two first-order symmetrically arranged V-shaped subglacial basins, the Wilkes (WSB) and Aurora (ASB) basins, which extend southward from the coastline for more than 1500 km with a predominantly north-south oriented main axis. However, east-west trending tectonic structures are also observed. The two main basins appear to be dissected by a system of transverse faults arranged along two circular belts, which we interpret as intraplate strike-slip shear belts[7], hereafter referred to as the southern and northern Transantarctic Circular strike-slip Shear Belts (Fig. 1). Along these belts, the Wilkes basin displays an apparent dextral offset whereas the Aurora basin shows an apparent sinistral offset. These features may reflect genuine strike-slip motion, or alternatively, a displacement of the extensional locus along pre-existing transverse structures. The two circular belts may be approximated on the Earth sphere by two small circles (Extended Data Fig. 2 and Methods) whose pole locations (sEP: 84.2°S, 130.8°E; nEP: 83.1°S, 129.5°E) are situated close to the fan pivot point EP, suggesting they were generated by the same process. Moreover, the Wilkes and Aurora basin bed elevation appears to be vertically offset across

the location of the two proposed strike-slip shear belts (Extended Data Fig. 3), suggesting a vertical component of displacement as well.

The coastline marking the northern limit of the EAFBP forms an arc of a circle. On average, it may be interpolated from Cape Adare to Prydz Bay by a small circle (Extended Data Fig. 2 and Methods) whose pole cEP is located at coordinates 81.7°S, 115.1°E, again close to the previously estimated poles EP, sEP, nEP. Consequently, the two shear belts and the coastline divide the EAFBP into three annuli that we name as the southern, central and northern Transantarctic Annuli. The two main Wilkes and Aurora basins cross all three annuli, while the other basins are confined within them.

The EAFBP is laterally delimited by two of the most least understood mountain ranges on Earth (Fig. 1). To the west, the Gamburtsev Mountains are an intraplate subglacial range of uncertain origin[8-11] that exhibit unexpectedly youthful Alpine topography[8]. To the east, the Transantarctic Mountains are the largest non-compressional mountain belt in the world[12] separating East Antarctica from the West Antarctic Rift System[13,14]. The Transantarctic Mountains are considered to be the uplifted shoulder of the West Antarctic Rift System, originating by thermal buoyancy of debated origin and timing and are divided into multiple deeply dissected tectonic blocks[12,21].

The structural connection between the EAFBP and the Transantarctic Mountains is clearly reflected in their topography.. Approximately at the same latitude of the southernmost vertex of the V-shaped Wilkes basin, between the Nimrod and Byrd glaciers, the Transantarctic Mountains exhibit a ~20° clockwise deflection relative to their southern linear trend. In addition, they appear segmented and right-laterally offset along both the Transantarctic Circular strike-slip Shear Belts forming three main distinct blocks (Fig. 1). Correspondingly, the West Antarctic Rift System grabens in the Ross Sea appear rotated clockwise[22] and right-laterally offset along the offshore continuation of the shear belts, even if there is no clear indication of effective right displacement along them.

The EAFBP onshore structure is also intriguingly reflected in the facing oceanic structures along the Southern Ocean between East Antarctica and Australia (Fig. 2). In fact, the oceanic fracture zones are more closely spaced and prominent in correspondence with the main onshore structural lineaments in the EAFBP: the Transantarctic Mountains and the Wilkes basin to the east and the Lambert rift, SB1, Sabrina and Aurora basins to the west. Analysis of ridge offset variations versus

longitude along the ridge (Fig. 2) confirms this observation and allow us to identify five oceanic ridge segments: i) the Transantarctic Mountains – Wilkes basin segment, showing the strongest offsets in correspondence with the Balleny (continuation of the discontinuity between the Transantarctic Mountains and the West Antarctic Rift System), the George V (in continuation of the western Wilkes basin margin) and Tasman (eastern Wilkes basin margin) fracture zones; ii) a central 'quiet' segment with very limited ridge offsets facing the Belgica bisector area; iii) the Sabrina-Aurora segment with a relevant but smoother distribution of the ridge offsets facing the two basins; iv) a second minor 'quiet' segment separating the westernmost v) Lambert-SB1 segment with increased fracture zone spatial density and offsets.

Geophysical observations

The different rheological properties of distinct intracontinental blocks[19,20,23] may have controlled the rotational extension within the EAFBP. The Lake Vostok trough is formed by a major geological boundary[24,25] apparent in magnetic and Bouguer gravity anomalies that is partially coincident with the proposed Mawson continent western flank[19] (Western Mawson Suture) that appears to delimit the Aurora basin to the west. The western flank of the Wilkes basin features a sharp magnetic[26,27] and gravimetric[28] break that defines the boundary (Eastern Mawson Suture) between the thick and highly magnetic Mawson continent[19,23,27] of the East Antarctic Cratonic Assemblage[29] and the thinner and weakly magnetic Ross Orogen Belt[23,26,27] (Fig. 2).

The fan-shaped structure is also recorded in the lithosphere. A crustal depth model[30], based on integrated seismic and gravimetric data, indicates thinned crust corresponding with the major basins in the EAFBP (Extended Data Fig. 4A) that we interpret as due to extension. At the same time, thinner lithosphere[31] (Extended Data Fig. 4B) has been observed in association with the identified basins, which result located between spoke-like structural culminations of the Lithosphere Asthenosphere Boundary linked to thicker lithosphere[4].

The kinematic model

Candidate processes that may have operated in the study area and generated the semi-continental scale fan-like structural pattern of the EAFBP include glacial erosion and extensional tectonic

deformation (e.g., rotational extension[32,33,34], rift propagation[35] and structural control by inherited structures[36]. We discount glacial erosion as the primary mechanism shaping the observed topography because contemporary ice surface velocities[37] across the study area (Extended Data Fig. 5) are widely low (<10 m/yr) and geomorphological evidence suggests that glacial erosion by earlier ice sheets in the East Antarctic interior was selectively focused through existing valleys on a smaller scale than the features comprising the EAFBP[38]. We also consider rift propagation mechanisms unlikely here because they typically affect spreading centres at mid-ocean ridges and back-arc basins[39]. Finally, we regard a deformation model relying exclusively on the guidance of inherited structures as unlikely as well, given that the well-defined north-south oriented radial patterns, extensively distributed over at least half of East Antarctica and converging unmistakably toward a single, well-defined pivot point, demand a fundamental genetic explanation.

We have therefore developed a conceptual kinematic model for the evolution of the EAFBP explaining the observations presented (summarized in Extended Data Tab. 2) based on the rotational extension mechanism, which has been extensively used to account for similar structural patterns widely observed elsewhere in the world[32-34,40-43]. In planar view, the process is analogous to the opening of a folding fan and so requires a pivot point and a fixed central arm from which the two sides of the fan are moved away (Extended Data Fig. 6). The resultant kinematic model is simplified in two phases sketched in Fig. 3.

At the initial stage (Fig. 3A), counter-clockwise fan-shaped extension around the pivot point EP formed the Aurora basin, while simultaneous clockwise extension formed the Wilkes basin. Both basins, with their characteristicV-shape, together defined a large sphenocasm[43] within the continental crust.

The fanning out (i.e., the rotational extension) propagated from the Belgica bisector, that represents its fixed arm while the basins master faults' locations were controlled by the existing lithospheric discontinuities made by the Eastern and Western Mawson sutures. In our model, the increasing deepening towards the north of the two basins along their master faults (Extended Data Fig. 6) was accommodated brittlely by two main east-west normal faults in the basement, possibly in coincidence with pre-existing east-west lithospheric discontinuities in the Neoproterozoic rift margin[20]. The western side of the Wilkes basin coincided partially with the Eastern Mawson Suture and remained unaffected by the following dextral offset. The eastern side of the Aurora basin

matched partially with the Western Mawson Suture and was likely affected by the following sinistral offset. As result, the Mawson continent evolved from an elongated stripe-shape to the final present-day V-shape.

Within the rotational extension framework, the ~20° deflection observed in the Transantarctic Mountains is interpreted as a rotation consistent with the position of the fan pivot point (EP). The deflection point is located between the Nimrod and Byrd glaciers, which likely coincide with the location of inherited main fault structures that accommodated the rotational extension by both vertical and strike-slip movements. The area corresponds to a previously observed but unexplained lithospheric discontinuity[22] in the Transantarctic Mountains and Ross Sea.

At a later stage (Fig. 3B), as the fan extension grew, the increasing basement lowering in the northernmost sectors of the fan was compensated by secondary basins/trenches opening in the central and northern annuli. The secondary basins/trenches opened between the two intraplate strike-slip deformation belts that were forming along the original east-west lithospheric breaks in the Wilkes and Aurora basins. Our model proposes that the original east-west lithospheric breaks in the Wilkes and Aurora basins acted, during this second phase of deformation, as zones of weakness along which transverse strike-slip movements developed, induced by the rotational extension itself. We have compiled a list of evidence (see Supplementary Information) suggesting that these east-west strike-slip movements, transverse to the basins, are likely, though not certain. We consider the conversion from normal to strike-slip deformation along the two belts necessary to accommodate the different amounts of extensional strain across the three annuli, which increase from south to north, likely differentiating them as observed in similar contexts[44,45]. Alternatively, the observed transverse offsets could be interpreted as transfer faults that shift the focus of extension without actual strike-slip motion, although we consider this explanation less probable.

The increasing extensional strain towards the North, accommodated along the shear belts, likely caused the segmentation of the Transantarctic Mountains into the three observed blocks (Fig. 1) and the corresponding segmentation of the extensional features in the West Antarctic Rift System. The three Transantarctic Mountains blocks overrode the West Antarctic Rift System hot lithosphere, and underwent additional differential uplift in time and space due to differential thermal buoyancy[12] (Extended Data Fig. 7). The southern Transantarctic circular strike-slip shear belt offsets the Transantarctic Mountains north of the Skelton Glacier, whereas the northern belt

offsets them in the area between David and Tucker glaciers. The locations of two major seismic low velocity zones detected in the mantle[46,47] appear to be likely controlled by these discontinuities.

To the west, rotational extension has only weakly affected the area beyond the Western Mawson Suture likely due to the originally thicker crust and lithosphere, as shown by crustal and Lithosphere-Asthenosphere Boundary depth maps[30,31] (Extended data Fig. 4). In this area extension was focused along deep and narrow trenches such as Lake Vostok and the East Antarctic Rift System. However, the fanning out likely reactivated the Lambert Rift and, in the later stage, offset the East Antarctic Rift System. We propose that the rotational extension in the EAFBP was, at least partially, accommodated by compression in the Gamburtsev Mountains region causing additional uplift and, thus, their observed youthful Alpine topography[8].

To the north, the EAFBP fanning out originated the semi-circular lithospheric weakness line that controlled Antarctica-Australia separation. In fact, in our model, the inferred EAFBP transcurrent releasing fault system representing the fan northern limit evolved from a semi-circular wide diffuse principal displacement zone to a set of strike-slip faults disposed en-èchelon (Fig. 4). The most prominent of these faults originated from the bending in the principal displacement zone of existing major lithospheric discontinuities (like the Eastern and Western Mawson sutures and the Transantarctic Mountains - West Antarctic Rift System discontinuity) and/or of the major longitudinal coastal basins' normal master faults.

At a later stage, all along the northern EAFBP edge, approximately east-west pull-apart basins developed between the consecutive overlapping strike-slip faults and might have evolved into short seafloor spreading segments with large offset between them. During the subsequent Antarctica/Australia rifting phase of the Gondwana breakup, the pull-apart basins drove the west to east propagation of the oceanic ridge causing the formation of the transfer faults that originated the present-day fracture zone distribution and the corresponding partitioning of the Southeast Indian Ridge in the five observed segments (Fig. 2). The final effect was the semi-circular trend of the present-day coastlines and ocean-continent boundaries at the conjugated Antarctic/Australian margins. The evident deviation towards north-west of the Eastern Mawson Suture at the coastline and a set of inferred strike-slip faults marked by canyons and scarps in the continental slope and platform facing the main fracture zones in the oceanic crust (Fig. 2) at both

the Antarctic/Australian margins may be considered the remaining evidence of the whole proposed process. We have compiled a comprehensive list of supporting evidence for the proposed mechanism in the Supplementary Information.

Timing of the rotational extension

The extensive glacial coverage preventing direct observations in the inner continent and the uncertainties about both the age and evolution of the Transantarctic Mountains and the West Antarctic Rift System[13,16-21] make it difficult to estimate when and how long the EAFBP was active. The rotational extension might have occurred during known tectonic plate re-arrangements or major extension episodes possibly triggering vast intracontinental sedimentary deposition across the East Antarctic interior (i) in the Late Paleozoic–Triassic when a major denudation event occurred[48], (ii) during Gondwana breakup in the Jurassic–Cretaceous and early Cenozoic[49] and/or (iii) the Eocene with possible transcurrent sinistral offsets along the eastern rift margin[50]. It must also be considered that the fanning out may have been superimposed on the intra-Gondwana Mesozoic Victoria Basin[16] and the possibility of multiphase asynchronous extension.

However, in the classical view that considers the modern Transantarctic Mountains uplift occurring mostly in the late Mesozoic and early Cenozoic as result of partially coeval extension in the West Antarctic Rift System[13,18-21] it is possible to constrain the timing of the EAFBP onset, at least for its dextral sector. In this scenario, the southern and northern Transantarctic Circular strike-slip Shear Belts are basement structures that offset late Mesozoic rift-graben axes in the West Antarctic Rift System[13,19,20] and similar age mountain topography along the Transantarctic Mountains[20,21], setting the oldest time limit for the process ($\lesssim$ 150 Ma?). At the same time, the EAFBP fanning out slightly preceded the propagation of the southern Australian - East Antarctic margin separation that broke up Gondwana progressively from West in the late Mesozoic to the East in the early Cenozoic[36,49,50] setting the youngest time limit for the process ($\gtrsim$ 30 Ma?).

Implications for the subsequent tectonic and glacial evolution of East Antarctica

According to the proposed model, the EAFBP large "handheld fan" shaped feature in the East Antarctic landscape originated by a single continental scale process driven by rotational extension.

This composite process profoundly reworked pre-existing structures and influenced the development of later continental scale features. It triggered additional uplift of the Gamburtsev and Transantarctic mountains, segmented the Transantarctic Mountains and the West Antarctic Rift System and guided the subsequent formation of the semicircular conjugated continental margins between Antarctica and Australia. As a result, it played a significant role in the Gondwana breakup, with major implications for global tectonic reconstructions and geodynamic models that seek to explain genetic links between onshore structures and offshore fracture zones. Crucially, our interpretation identifies east-west rotational extensional movements as a fundamental precursor to the opening of the oceanic rift between Australia and East Antarctica. Furthermore, the approximate coincidence between the fan's pivot pole and the Euler poles proposed for East/West Antarctica extension[51] after ~34 Ma (Extended Data Fig 2), when uncertainties in pole location are taken into account, raises intriguing questions about the long-term stability of deformation poles and their potential role in linking continental rifting processes to subsequent plate motions.Since no evidence of the EAFBP continuation is found in Australia, the fan-like rotational extension must have been confined to the Antarctic plate. Consequently, this intra-plate deformation is expected to strongly affect new plate reconstructions of the Australia-Antarctica fit, potentially accounting for the anomalously large crustal overlaps reported in some models[52,53] and for mismatches in the correlation of basement terranes and major faults across the two opposing conjugate margins[49,54].

Also, the proposed tectonic scenario may have significantly influenced the onset and evolution of the East Antarctic Ice Sheet that nucleated at about 34 Ma. Over the EAFBP region, the volume of ice has a sea level equivalent of 28 m. Sedimentary basins interact with the overlying ice sheet through dynamic feedbacks that are known to impact ice-sheet retreat dynamics[3,4]. The segmentation of the Transantarctic Mountains along the east-west circular shear belts was likely subsequently exploited by major outlet glaciers (e.g., Byrd, Beardmore, Nimrod), incising particularly deep glacial troughs that in turn caused further isostatic uplift of the mountain peaks. Similarly, the major north-south fan shaped structural boundaries of the basins within the EAFBP appear to control the locations of major outlet glaciers around the East Antarctic margin (e.g., Totten, Vanderford, Denman, Frost, Amery). The implications of this association are the direct tectonic control on the behavior of the ice sheet throughout its existence, and the importance of

geological processes that commenced ~ 150 hundreds million years ago in modulating ice sheet dynamics today and in the future.

Data availability

The filtered rebounded topography and detected lineaments shown in this work are available at https://figshare.com/s/7d6edac6f4d885663034. The Antarctic bed topography is available at: M. Morlighem (2022). MEaSUREs BedMachine Antarctica, Version 3 [Data Set]. Boulder, Colorado USA. NASA National Snow and Ice Data Center Distributed Active Archive Center. https://doi.org/10.5067/FPSU0V1MWUB6. The rebounded Antarctic bed topography is available at: G. Paxman, J. Austermann, A. Hollyday (2022). Grid files of the total isostatic response to the complete unloading of the Greenland and Antarctic Ice Sheets (version 1). Arctic Data Center. https://doi.org/10.18739/A2280509Z. The ETOPO global relief model is available at: NOAA National Centers for Environmental Information (2022). ETOPO 2022 15 Arc-Second Global Relief Model. NOAA National Centers for Environmental Information. https://doi.org/10.25921/fd45-gt74. The GEOMAP data set is available at: S.C. Cox et al., The GeoMAP (v.2022-08) continent-wide detailed geological dataset of Antarctica. PANGAEA (2023), https://doi.org/10.1594/PANGAEA.951482. The MEaSUREs Antarctic ice velocity data set is available at: Mouginot, J., E. Rignot, and B. Scheuchl. 2019. MEaSUREs Phase-Based Antarctica Ice Velocity Map, Version 1. Boulder, Colorado USA. NASA National Snow and Ice Data Center Distributed Active Archive Center. https://doi.org/10.5067/PZ3NJ5RXRH10. The MEaSUREs Antarctic ice basin divides are available at: Mouginot, J., B. Scheuchl, and E. Rignot. 2017. MEaSUREs Antarctic Boundaries for IPY 2007-2009 from Satellite Radar, Version 2. Boulder, Colorado USA. NASA National Snow and Ice Data Center Distributed Active Archive Center. https://doi.org/10.5067/AXE4121732AD. The aeromagnetic ADMAP2 data set is

available at: A. V. Golynsky et al., (2018): ADMAP2 Magnetic anomaly map of the Antarctic - links to files. PANGAEA, https://doi.org/10.1594/PANGAEA.892724

Code availability

Scripts used to support the analysis of topographic data are available at https://figshare.com/s/7d6edac6f4d885663034.

Author contributions:

Conceptualization: EA

Methodology: EA, DR, PB, AG, DS, GP, AZ

Investigation: EA, DR, PB, AG, DS, AZ

Visualization: EA, DR, PB, AG, DS, AZ

Funding acquisition: EA, LC, FF, AL

Supervision: MS, EA, AZ, GP, FF, LC, AL, FL, AR, DM

Writing – original draft: EA

Writing – review & editing: all

Competing interests

Authors declare that they have no competing interests.

References (main text)

1. Frémand, A.C. et al. Antarctic Bedmap data: FAIR sharing of 60 years of ice bed, surface and thickness data. *Earth System Science Data* **15**, 2695–2710 (2023), doi:10.5194/essd-15-2695-2023
2. Morlighem, M. et al. Deep glacial troughs and stabilizing ridges unveiled beneath the margins of the Antarctic ice sheet. *Nature Geoscience* **13**, 132-137 (2020), doi:10.1038/s41561-019-0510-8
3. Li, L., Aitken, A.R.A., Lindsay, M.D., Mark D.L. & Kulessa, B. Sedimentary basins reduce stability of Antarctic ice streams through groundwater feedbacks. *Nat. Geosci.* **15**, 645–650 (2022). https://doi.org/10.1038/s41561-022-00992-5
4. Aitken, A.R.A. et al. Antarctic sedimentary basins and their influence on ice-sheet dynamics. *Reviews of Geophysics* **61**, e2021RG000767 (2023), doi:10.1029/2021RG000767
5. Li, L., & Aitken, A.R.A. Crustal heterogeneity of Antarctica signals spatially variable radiogenic heat production. Geophysical Research Letters **51** (2024), e2023GL106201. https://doi.org/10.1029/2023GL106201
6. Paxman, G.J.G. et al. Bedrock erosion surfaces record former East Antarctic Ice Sheet extent. *Geophysical Research Letters* **45**, 4114–4123 (2018), doi:10.1029/2018GL077268
7. Storti, F., Holdsworth, R. E., Salvini, F. "Intraplate Strike-Slip Deformation Belts" in Intraplate Strike-Slip Deformation Belts, F. Storti, R. E. Holdsworth, F. Salvini, Eds., *Geological Society of London* (2003), pp. 1–14, doi:10.1144/gsl.sp.2003.210.01.01
8. Bo, S. et al. The Gamburtsev mountains and the origin and early evolution of the Antarctic Ice Sheet. *Nature* **459**, 690–693 (2009), doi:10.1038/nature08024
9. Ferraccioli F. et al. East Antarctic rifting triggers uplift of the Gamburtsev Mountains. *Nature* **479**, 388–392 (2011), doi:10.1038/nature10566.
10. Lisker, F., Brown, R., Fabel, D. Denudational and thermal history along a transect across the Lambert Graben, northern Prince Charles Mountains, Antarctica, derived from apatite fission track thermochronology. *Tectonics* **22**, 1055 (2003), doi:10.1029/2002TC001477
11. Phillips, G. & Läufer, A.L. Brittle deformation relating to the Carboniferous-Cretaceous evolution of the Lambert Graben, East Antarctica: A precursor for Cenozoic relief development in an intraplate and glaciated region. *Tectonophysics* **471**, 216–224 (2009), doi:10.1016/j.tecto.2009.02.012
12. Smith, A. & Drewry, D. Delayed phase change due to hot asthenosphere causes Transantarctic uplift? *Nature* **309**, 536–538 (1984), doi:10.1038/309536a0
13. Behrendt, J.C. Crustal and lithospheric structure of the West Antarctic Rift System from geophysical investigations - a review. *Global and Planetary Change* **23**, 25-44 (1999), doi:10.1016/S0921-8181(99)00049-1.
14. Granot, R. & Dyment, J. Late Cenozoic unification of East and West Antarctica. *Nat. Commun.* **9**, 3189 (2018), doi:10.1038/s41467-018-05270-w
15. Paxman G.J.G. et al. The role of lithospheric flexure in the landscape evolution of the Wilkes Subglacial Basin and Transantarctic Mountains, East Antarctica. *Journal of Geo-physical Research. Earth Surface* **124**, 812–829 (2019), doi:10.1029/2018JF004705
16. Lisker, F. & Läufer, A.L. The Mesozoic Victoria Basin: Vanished link between Antarctica and Australia. *Geology* **41**, 1043–1046 (2013), doi:10.1130/G33409.1
17. Prenzel, J. et al. Development and inversion of the Mesozoic Victoria Basin in the Terra Nova Bay (Transantarctic Mountains) derived from thermochronological data. *Gondwana Research* **53**, 110-128 (2018), doi:10.1016/j.gr.2017.04.025.
18. Baldwin, S.L., Fitzgerald, P.G., Malusà, M.G. "Crustal exhumation of plutonic and meta-morphic rocks: constraints from fission-track thermochronology" in Fission-track thermochronology and its application to geology, M.G. Malusà, P.G. Fitzgerald, Eds., *Springer, Berlin* (2018), pp. 235-257, doi:10.1007/978-3-319-89421-8_13
19. Siddoway, C. "Antarctica" in Encyclopedia of Geology, 2nd edition, S.A. Elias, D. Alderton, Eds., *Academic Press* (2021), pp. 642-658, doi:10.1016/B978-0-08-102908-4.00136-3
20. Goodge, J.W. Geological and tectonic evolution of the Transantarctic Mountains, from ancient craton to recent enigma. *Gondwana Research* **80**, 50-122 (2020), doi:/10.1016/j.gr.2019.11.001.
21. Faure, G. & Mensing, T.M. The Transantarctic Mountains: Rocks, Ice, Meteorites and Water, *Springer* (2011).

22. Cooper, A.K., Davey, F.J., Hinz, K. "Crustal extension and origin of sedimentary basin be-neath the Ross Sea and Ross Ice Shelf, Antarctica" in Geological Evolution of Antarctica, M.R.A Thompson, J.A. Crame, J.W. Thompson, Eds., *Cambridge Univ. Press, New York* (1991), pp. 285-291

23. Boger, S.D. Antarctica - Before and after Gondwana. *Gondwana Research* **19**, 335-371 (2011), doi:10.1016/j.gr.2010.09.003.

24. Studinger, M. t al. Geophysical models for the tectonic framework of the Lake Vostok region, East Antarctica. *Earth Planet. Sci. Lett.* **216**, 663-677 (2003), doi:10.1016/S0012-821X(03)00548-X

25. Leonov, V.O. & Popov, S.V. Geological Structure of Central East Antarctica from Geophysical Data. *Geotectonics* **43**, 274–282 (2009).

26. Ferraccioli, F., Armadillo, E., Jordan, T., Bozzo, E., Corr, H. Aeromagnetic exploration over the East Antarctic Ice Sheet: a new view of the Wilkes Subglacial Basin. *Tectonophysics* **478**, 62-77 (2009), doi: 10.1016/j.tecto.2009.03.013

27. Golynsky, A.V. et al., New magnetic anomaly map of the Antarctic. *Geophysical Research Letters* **45**, 6437–6449 (2018), doi:10.1029/2018GL078153

28. Jordan, T.A., Ferraccioli, F., Armadillo, E., Bozzo, E. Crustal architecture of the Wilkes Subglacial Basin in East Antarctica, as revealed from airborne gravity data. *Tectonophysics* **585**, 196–206 (2013), doi:10.1016/j.tecto.2012.06.041.

29. Ruppel, A.S. et al., The Main Shear Zone in Sør Rondane, East Antarctica: Implications for the late-Pan-African tectonic evolution of Dronning Maud Land. *Tectonics* **34**, 1290–1305 (2015), doi:10.1002/2014TC003763.

30. Baranov, A., Tenzer, R. & Morelli, A. Updated Antarctic crustal model. *Gondwana Research* **89**, 1–18 (2021), doi:10.1016/j.gr.2020.08.010

31. An, M. et al., Temperature, lithosphere-asthenosphere boundary, and heat flux beneath the Antarctic Plate inferred from seismic velocities, *J. Geophys. Res. Solid Earth* **120**, 8720–8742 (2015), doi:10.1002/2015JB011917

32. Zwaan, F., Schreurs, G. & Rosenau, M. Rift propagation in rotational versus orthogonal extension: Insights from 4D analogue models. *Journal of Structural Geology* **135**, 103946 (2020), doi:10.1016/j.jsg.2019.103946

33. Zwaan, F. & Schreurs, G. Rift segment interaction in orthogonal and rotational extension experiments: Implications for the large-scale development of rift systems. *Journal of Structural Geology* **140**, 104119 (2020), doi:10.1016/j.jsg.2020.104119.

34. Schmid, T.S., Schreurs, G. & Adam, J. Characteristics of continental rifting in rotational systems: New findings from spatio temporal high resolution quantified crustal scale analogue models. *Tectonophysics* **822**, 229174 (2022), doi:10.1016/j.tecto.2021.229174

35. Kundu, B., Zwaan, F. & Senapati, B. Unfolding rotational tectonics and topographic evolution from localized verses diffuse plate boundary counterparts. *Sci. Rep.* **14**, 8199 (2024). https://doi.org/10.1038/s41598-024-58921-y

36. Gibson, G. M., et al., Pre-existing basement structure and its influence on continental rifting and fracture zone development along Australia's southern rifted margin. *Journal of the Geological Society, London* **170**, 365–377 (2013). doi: 10.1144/jgs2012-040

37. Mouginot, J., Rignot, E. & Scheuchl, B. Continent-wide, interferometric SAR phase-mapping of Antarctic ice velocity. Geophysical Research Letters **46** (2019). DOI: 10.1029/2019GL083826.

38. Jamieson, S.S.R., Sugden, D.E. & Hulton, N.R.J. The evolution of the subglacial landscape of Antarctica. Earth and Planetary Science Letters **293**, 1–2, 1-27 (2010), https://doi.org/10.1016/j.epsl.2010.02.012.

39. Parnell-Turner, R. & al. Causes and consequences of diachronous V-shaped ridges in the North Atlantic Ocean. Journal of Geophysical Research: Solid Earth **122**, 8675–8708 (2017). https://doi.org/10.1002/2017JB014225

40. Mondy, L.S., Rey, P.F., Duclaux, G. & Moresi, L. The role of asthenospheric flow during rift propagation and breakup. *Geology* **46**, 103–106 (2017), doi:10.1130/G39674.1

41. Maestrelli, D. et al. Exploring the interactions between rift propagation and inherited crustal fabrics through experimental modeling. *Tectonics* **39**, e2020TC006211 (2020). doi:10.1029/2020TC006211

42. Molnar, N. E., Cruden, A. R. & Betts, P. G. Interactions between propagating rotational rifts and linear rheological heterogeneities: Insights from three-dimensional laboratory experiments. *Tectonics* **36**, 420–443 (2017), doi:10.1002/2016TC004447.

43. Carey, S. W. The orocline concept in geotectonics. *Proc. Royal Soc. Tasmania* **89**, 255–288 (1955).

44. Trench, D., Meigs, A. & Grunder, A. Termination of the northwestern Basin and Range province into a clockwise rotating region of transtension and volcanism, southeast Oregon. *Journal of Structural Geology* **39**, 52-65 (2012), https://doi.org/10.1016/j.jsg.2012.03.007.

45. Villamor, P. et al. Rapid evolution of subduction-related continental intraarc rifts: The Taupo Rift, New Zealand. *Tectonics* **36**, 2250–2272 (2017). https://doi.org/10.1002/2017TC004715

46. Graw, J.H. et al. Upper mantle shear wave velocity structure beneath northern Victoria Land, Antarctica: Volcanism and uplift in the northern Transantarctic Mountains. *Earth and Planetary Science Letters* **449**, 48–60 (2016), doi:10.1016/j.epsl.2016.05.026

47. Hansen, S.E., Kenyon, L.M., Graw, J.H., Park, Y. & Nyblade, A.A. Crustal structure beneath the Northern Transantarctic Mountains and Wilkes Subglacial Basin: Implications for tectonic origins. *Journal of Geophysical Research* **121**, 812–825 (2016), doi:10.1002/2015JB012325

48. Maritati, A., Danišík, M., Halpin, J. A., Whittaker, J. M., & Aitken, A. R. A. Pangea rifting shaped the East Antarctic landscape. Tectonics **39**, (2020), e2020TC006180. https://doi.org/10.1029/2020TC006180

49. Williams, S.E. et al. Australian-Antarctic breakup and seafloor spreading: Balancing geological and geophysical constraints. *Earth-Science Reviews* **188**, 41-58 (2019), doi:10.1016/j.earscirev.2018.10.011.

50. Eagles, G. A little spin in the Indian Ocean plate circuit. *Tectonophysics* **754**, 80-100 (2019), doi:10.1016/j.tecto.2019.01.015

51. Granot, R., Cande, S. C., Stock, J. M. & Damaske, D. Revised Eocene-Oligocene kinematics for the West Antarctic rift system. *Geophys. Res. Lett.* **40**, 279–284 (2013). https://doi.org/10.1029/2012GL054181

52. Tikku, A.A. & Cande, S.C. The oldest magnetic anomalies in the Australian-Antarctic Basin: Are they isochrons? *J. Geophys. Res.* **104(B1)**, 661–677 (1999), doi:10.1029/1998JB900034.

53. Jacob, J. & Dyment, J. Early opening of Australia and Antarctica: New inferences and regional consequences. *Tectonophysics* **636**, 244-256 (2014), doi:10.1016/j.tecto.2014.08.020

54. White, L.T., Gibson, G.M. & Lister, G.S. A reassessment of paleogeographic reconstructions of eastern Gondwana: Bringing geology back into the equation. *Gondwana Research* **24**, 984-998 (2013), doi:10.1016/j.gr.2013.06.009.

55. Paxman, G.J.G., Austermann, J. & Hollyday, A. Total isostatic response to the complete unloading of the Greenland and Antarctic Ice Sheets. *Sci. Rep.* **12**, 11399 (2022), doi:10.1038/s41598-022-15440-y

56. Decesari, R.C., Wilson, D.S., Luyendyk, B.P., Faulkner, M. Cretaceous and Tertiary extension throughout the Ross Sea, Antarctica. *USGS Short Research Paper* **098**, USGS OF-2007-1047 (2007), doi:0.3 33/of2007-1047.srp098

57. Cox, S.C. et al. A continent-wide detailed geological map dataset of Antarctica. *Sci. Data* **10**, 250 (2023), doi:10.1038/s41597-023-02152-9

58. Wilson, T.J. Cenozoic structural segmentation of the Transantarctic Mountains rift flank in southern Victoria Land. *Global and Planetary Change* **23**, 105-127 (1999), doi:10.1016/S0921-8181(99)00053-3.

59. Matthews, K.J., Müller, R.D., Wessel, P. & Whittaker, J.M. The tectonic fabric of the ocean basins. *J. Geophys. Res.* **116**, B12109 (2011), doi:10.1029/2011JB008413

60. Wolfson-Schwehr, M., Boettcher, M.S. "Global Characteristics of Oceanic Transform Fault Structure and Seismicity" in Transform Plate Boundaries and Fracture Zones, J.C. Duarte, Ed., *Elsevier* (2019), pp. 21-59, doi:10.1016/B978-0-12-812064-4.00002-5

61. NOAA National Centers for Environmental Information, ETOPO 2022 15 Arc-Second Global Relief Model. *NOAA National Centers for Environmental Information* (2022). doi: 10.25921/fd45-gt74

62. Gaina, C., Müller, R.D., Brown, B., Ishihara, T. & Ivanov, S. Breakup and early seafloor spreading between India and Antarctica. *Geophysical Journal International* **170**, 151–169 (2007), doi:10.1111/j.1365-246X.2007.03450.x

63. Müller, R.D. et al. A global plate model including lithospheric deformation along major rifts and orogens since the Triassic. *Tectonics* **38**, 1884–1907 (2019), doi:10.1029/2018TC005462

64. Seton, M. et al. A global data set of present-day oceanic crustal age and seafloor spreading parameters. *Geochemistry, Geophysics, Geosystems* **21**, e2020GC009214 (2020), doi:10.1029/2020GC009214

65. Müller, R.D. et al. Ocean basin evolution and global-scale plate reorganization events since Pangea breakup. *Annual Review of Earth and Planetary Sciences* **44**, 107-138 (2016), doi:10.1146/annurev-earth-060115-012211.

.

References (Methods, Extended Data and Supplementary Information)

66. Morlighem, M. MEaSUREs BedMachine Antarctica. (NSIDC-0756, Version 3). Boulder, Colorado USA. NASA National Snow and Ice Data Center Distributed Active Archive Center. https://doi.org/10.5067/FPSU0V1MWUB6.

67. Portniaguine, O. & Zhdanov, M.S. Focusing geophysical inversion images. *Geophysics* **64**, 874-887 (1999), doi:10.1190/1.1444596

68. Kovesi, P., Image features from phase congruency. *Videre: A Journal of Computer Vision Research* **1(3)**, article 1 (1999).

69. Ghirotto, A. et al. The sub-ice structure of Mt. Melbourne Volcanic Field (Northern Victoria Land, Antarctica) uncovered by high-resolution aeromagnetic data. *Journal of Geophysical Research: Solid Earth* **128**, e2022JB025687 (2023), doi:10.1029/2022JB025687

70. Delaunay, A. et al. Structure and morphology of the Red sea, from the mid-ocean ridge to the ocean-continent boundary. *Tectonophysics* **849**, 229728 (2023), doi:10.1016/j.tecto.2023.229728

71. Milia, A., Torrente, M.M. & Tesauro, M. From stretching to mantle exhumation in a triangular backarc basin (Vavilov basin, Tyrrhenian Sea, Western Mediterranean), *Tectonophysics* **710–711**, 108-126 (2017), doi:10.1016/j.tecto.2016.10.017.

72. Federico, L., Crispini, L. & Capponi, G. Fault–slip analysis and transpressional tectonics: a study of Paleozoic structures in northern Victoria Land, Antarctica. *Journal of Structural Geology* **32**, 667-684 (2010), doi:10.1016/j.jsg.2010.04.001.

73. Cianfarra, P. et al., Multiple reactivations of the Rennick Graben Fault system (northern Victoria Land, Antarctica): New evidence from paleostress analysis. *Tectonics* 41, e2021TC007124 (2022), doi:10.1029/2021TC007124

74. Drewry, D.J. Sedimentary basins of the East Antarctic craton from geophysical evidence. *Tectonophysics* **36**, 301-314 (1976), doi:10.1016/0040-1951(76)90023-8

75. Drewry, D.J. Antarctica: Glaciological and Geophysical Folio. Scott Polar Res. Inst., University of Cambridge (1983).

76. Siegert, M.J., Carter, S., Tabacco, I., Popov, S. & Blankenship, D. A revised inventory of Antarctic subglacial lakes. *Antarct. Sci.* **17**, 453–460 (2005) doi:10.1017/S0954102005002889

77. Aitken, A.R.A. et al. The subglacial geology of Wilkes Land, East Antarctica. *Geophys. Res. Lett.* **41**, 2390–2400 (2014), doi:10.1002/2014GL059405.

78. Ravich, G.M., Soloviev, D.S. & Fodorov, L.V. Geologicheskoie Stroienie Zemli Mak-Robertsona (Vostochnaia Antarctida). *Gidrometoizdat* (1978)

79. An, M. et al. S-velocity model and inferred Moho topography beneath the Antarctic Plate from Rayleigh waves. *J. Geophys. Res. Solid Earth* **120**, 359–383 (2015), doi:10.1002/2014JB011332.

80. Fitzgerald, P.G. Tectonics and landscape evolution of the Antarctic plate since the breakup of Gondwana, with an emphasis on the West Antarctic Rift System and the Transantarctic Mountains. In: Gamble, J., Skinner, D.A., Henrys, S. (Eds.), Antarctica at the Close of a Millennium, Proceedings of the 8th International Symposium on Antarctic Earth Science: Wellington. Royal Society of New Zealand Bulletin **35**, 453–469 (2002)

81. Heimann, A., T.H. Fleming, D.H. Elliot, K.A. Foland. A short interval of Jurassic continental flood basalt volcanism in Antarctica as demonstrated by 40Ar39Ar geochronology. *Earth and Planetary Science Letters* **121**, 1–2 (1994). https://doi.org/10.1016/0012-821X(94)90029-9

82. Storti, F., Rossetti, F., Salvini, F. 2001. Structural architecture and displacement accommodation mechanisms at the termination of the Priestley Fault, northern Victoria Land, Antarctica. Tectonophysics, Volume 341, Issues 1–4, https://doi.org/10.1016/S0040-1951(01)00198-6

83. Foley, D. J. et al. "Differential Movement across Byrd Glacier, Antarctica, as indicated by Apatite (U–Th)/He thermochronology and geomorphological analysis". In Antarctic Palaeoenvironments and Earth-Surface Processes, M. J. Hambrey, P. F. Barker, P. J. Barrett, V. Bowman, B. Davies, J. L. Smellie, M. Tranter. *Geological Society, London, Special Publications* **381**, 37-43 (2013). https://doi.org/10.1144/SP381.25

84. Salvini, F. et al. Cenozoic geodynamics of the Ross Sea region, Antarctica: Crustal extension, intraplate strike-slip faulting, and tectonic inheritance. *Journal of Geophysical Research* **102**, B11. https://doi.org/10.1029/97JB01643

85. Rossetti, F., Storti, F. and Salvini, F. Cenozoic non-coaxial transtension along the western shoulder of the Ross Sea, Antarctica, and the emplacement of McMurdo dyke arrays, *Terra Nova* **12**, 60–66 (2000). https://doi.org/10.1111/j.1365-3121.2000.00270.x

86. Cianfarra, P. & Salvini, F. Intraplate Transtensional Tectonics in the East Antarctic Craton: Insight from Buried Subglacial Bedrock in the Lake Vostok-Dome C Region. *International Journal of Geosciences* **4**, 1275-1284 (2013). http://dx.doi.org/10.4236/ijg.2013.49122

87. Siegert, M., Popov, S. & Studinger, M. "Subglacial Lake Vostok: a review of geophysical data regarding its physiographical setting". In Subglacial Antarctic Aquatic Environments (M. Siegert, C. Kennicutt, B. Bindschadler, eds.), *AGU Geophysical Monograph* **192**. Washington DC, 45-60 (2011). 10.1029/2010GM000934

88. Wingham, D.J., Siegert, M.J., Shepherd, A.P. & Muir, A.S. Rapid discharge connects Antarctic subglacial lakes. *Nature* **440**, 1033-1036 (2006). https://doi.org/10.1038/nature04660

89. Yan, S. et al. A newly-discovered subglacial lake in East Antarctica likely hosts a valuable sedimentary record of ice and climate change. *Geology* , (2022). https://doi.org/10.1130/G50009.1

90. Pattyn, F. & Morlighem, M. The uncertain future of the Antarctic Ice Sheet. *Science* **367**, 1331-1335 (2020). DOI:10.1126/science.aaz5487
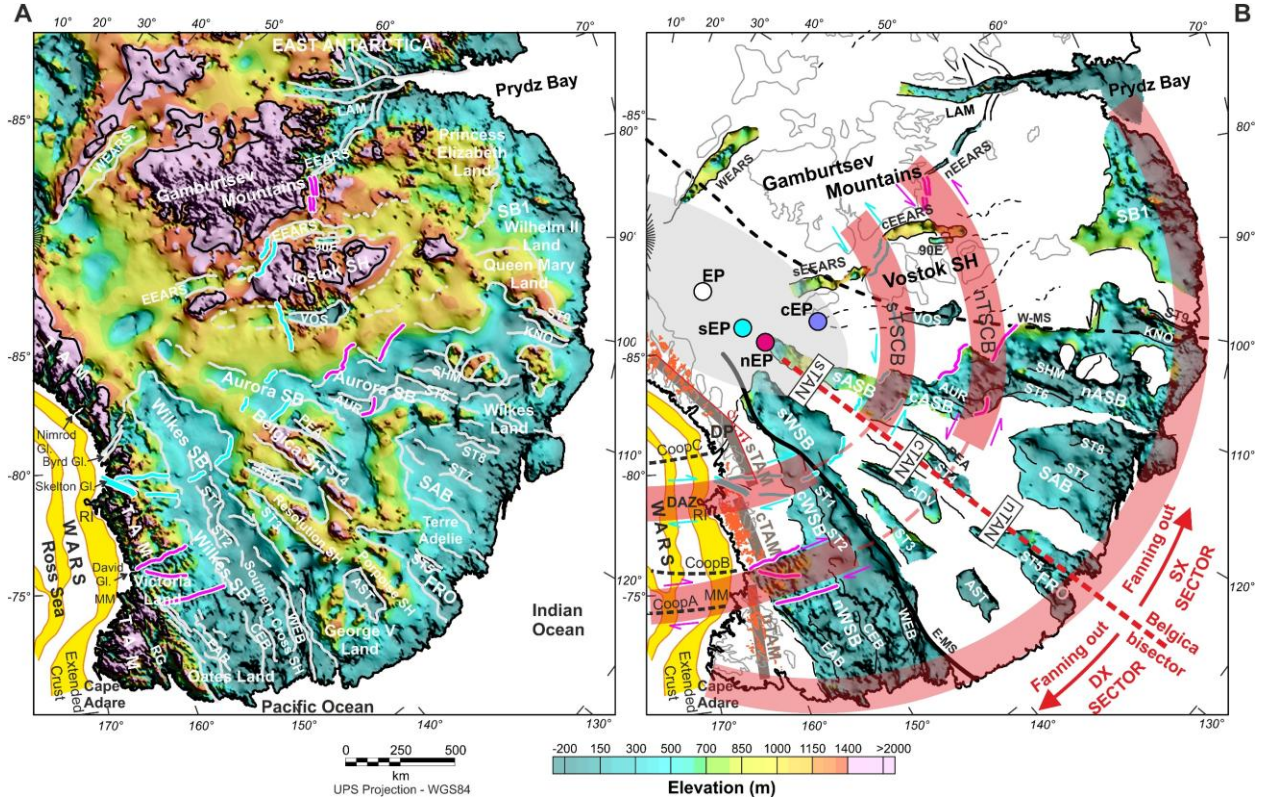
Figure 1. Fault-controlled basins and interpreted structural frame in the newly identified East Antarctic Fan Basin Province.

(A) Sub-ice topography corrected for isostatic rebound due to ice removal[55] with sharp topographic features enhanced by non-linear filtering (Methods). Light gray lines are detected topographic lineaments interpreted as longitudinal normal faults forming the structural edges of the basins. Magenta and cyan lines are detected topographic lineaments interpreted as either transverse strike-slip faults or associated normal faults that characterize the two circular shear belts sTCSB and nTCSB shown in (B). The acronyms of the basins are listed in Extended Data Tab. 1. The yellow bands in the Ross Sea outline highly-extended crust mapped from depth to basement and gravity anomalies[56]. Black contour line represents 1500 m elevation. MM: Mount Melbourne. RI: Ross Island. RG: Rennick Graben. WARS: West Antarctic Rift System.

(B) Main structural features of the East Antarctic Fan Basin Province. sTCSB, nTSCP: principal displacement zone of the southern and northern Transantarctic Circular strike-slip Shear Belts. sTAN, cTAN, nTAN: southern, central and northern Transantarctic Annuli. EP, sEP, nEP, cEP: estimated Euler pole from the edges of the basins (EP, error ellipse in light gray), from the structures associated to the sTCSB (sEP) and nTSCP (nEP) and from the coastline (cEP) between

Cape Adare and Prydz Bay ([Methods](#)). CoopA, CoopB, CoopC: mapped major lithospheric discontinuities s in the Ross Sea[22]. DP: deflecting point of the Transantarctic Mountains (TAM) indicating rotation with respect to their southern original trend. α: clockwise TAM rotation angle of about 20°. sTAM, cTAM, nTAM: TAM blocks formed by the offset along the sTCSB and nTSCP. E-MS: magnetic and gravimetric signature of the Eastern Mawson Suture[26,27]. W-MS: inferred Western Mawson Suture[19,57]. DAZ: Discovery accommodation zone[58]. Orange dots indicate outcrops of the Jurassic Ferrar Supergroup[57] that appear offset and rotated in three blocks as the TAM. Grey contour line represents 1500 m topographic elevation.
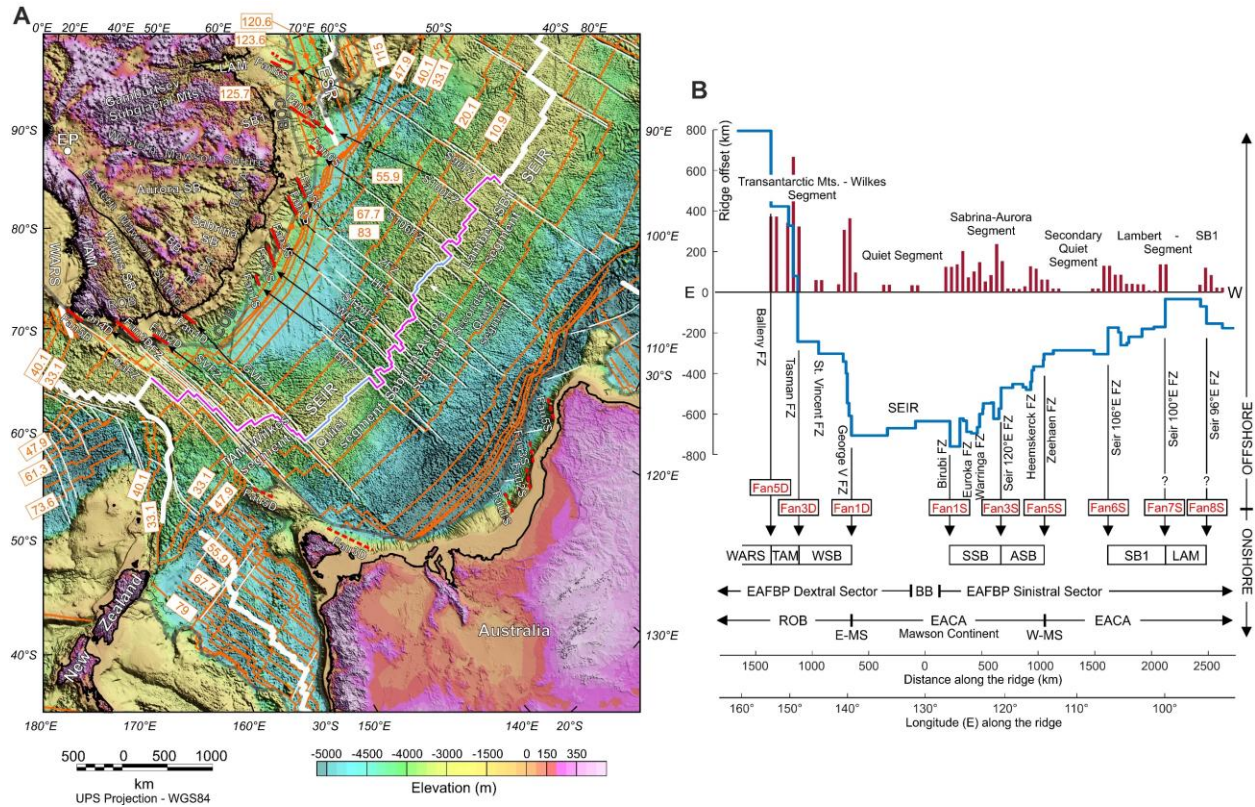
Figure 2. Offshore distribution and offsets of the fracture zones affecting the rifted margin between Antarctica and Australia with respect to the onshore location of the coastal basins forming the EAFBP.

(A) Present day configuration of the Antarctica-Australia rifted margin and main fracture zones[59,60] superimposed on the ETOPO Global Relief Model[61]. The correspondence of the offshore fracture zones (FZ) with the onshore coastal EAFBP basins' margins is obtained prolonging the FZ towards the Antarctic passive continental margin. Fan1D-Fan5D, Fan1S-Fan8S: canyons and scarps in the East Antarctica continental slope with a different trend than the maximum slope direction, interpreted here as indication of the remanence of the strike-slip faults forming the EAFBP northern transcurrent release fault system ([Fig. 4](#)). Fau1D-Fau5D, Fau1S-Fau8S: tentatively inferred continuations on the Australian margin of the Antarctic strike-slip Fan fault system. SEIR: Southeast Indian Ridge. ESR: extinct spreading ridge[62]. BaFZ: Balleny FZ; TFZ: Tasman FZ; SVFZ: St Vincent FZ; GVFZ: George V FZ; BiFZ: Birubi FZ; EFZ: Euroka FZ; WFZ: Warringa FZ; S120FZ: Seir120E FZ; HFZ: Heemskerck FZ; ZFZ: Zeehaen FZ; S106 FZ: Seir106E FZ; S100FZ: Seir100E FZ; S96FZ: Seir96E FZ. White thick lines: oceanic ridges[63]; white thin lines: main fracture zones[59]; orange lines: isochrons[64], years reported in Ma; thick gray lines: continental ocean boundaries[65]. COB: continent-ocean boundary. TAM: Transantarctic Mountains. WARS: West Antarctic Rift System. EACA: East Antarctic Cratonic Assemblage; ROB: Ross Orogen belt. Note that the relationship between the faults Fan7S and Fan8S with Seir100E and Seir96E FZs is more uncertain due to the greater distance between them.

(B) Blue line: SEIR offsets[63] along the fracture zones vs. the distance along the ridge; the zero of the offset scale is arbitrary, the zero of the distance along the ridge is the Belgica bisector (BB). Dark red lines: histogram representing the sum of the absolute values of the ridge offsets computed over a running window 100 km long with 50% of overlap between consecutive windows; bars are therefore proportional to the SEIR offset for unit distance. W-MS, E-MS: Western and Eastern Mawson sutures. Note the larger offsets of the SEIR in correspondence with the onshore EAFBP basins' limit in the continental crust. Also note the large difference in the offsets' trend for the FZs facing the onshore EACA and ROB domains and the consequent difference in the curvature of the coastline and COB.
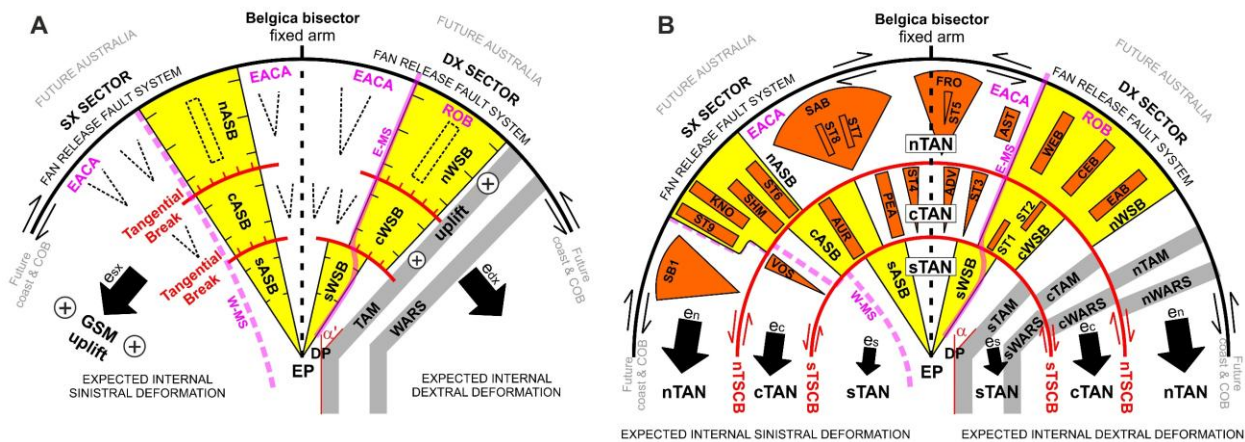
Figure 3. Cartoon showing the two-phase kinematic conceptual model of the EAFBP fanning out (not in scale).

(A) Initial phase with the formation of the major 'twin' Aurora and Wilkes basins caused by rotational movements around the Euler pole EP, symmetrical with respect to the Belgica bisector. Tangential normal faults (thick red lines) are formed in the two basins to accommodate the northward increasing depth. The Transantarctic Mountains (TAM) and the West Antarctic Rift System (WARS) are rotated clockwise by an angle α'. The extensional strain is higher in the dextral sector than in the sinistral sector ($e_{dx} > e_{sx}$), resulting in the different curvature of the continent-ocean boundary (COB) and the coastline as shown in detail in Fig. 4. Secondary basins (V-shaped and rectangular basins, dashed lines) open in the external annuli of the fan, to maintain the basin distribution for unit area approximately constant. To the west, the extension is accommodated by compressional reactivation of the Gamburtsev Mountains (GSM) uplift, which also occurs in the later phase. To the east, the TAM are pushed over the hot WARS lithosphere and undergo differential uplift (Extended Data Fig. 7). In this phase the Western Mawson Suture (W-MS) is bended anticlockwise; the Eastern Mawson Suture (E-MS) preserves its original orientation owing to its closeness to the Belgica fixed arm. EACA: East Antarctic Cratonic Assemblage; ROB: Ross Orogen belt; E-MS: Eastern Mawson Suture; W-MS: Western Mawson Suture; DP: TAM deflection point.

(B) Later phase with increasing opening of additional secondary basins and start-up of the lateral offsets along the southern and northern Transantarctic Circular strike-slip Shear Belts (sTCSB and nTSCP). The fan is divided into two sectors with dextral (DX) or sinistral (SX) shear and three annuli (the southern, sTAN, central, cTAN, and northern, nTAN, Transantarctic Annuli). The additional extensional strain increases in the three annuli from south to north ($e_s < e_c < e_n$). The shear along the three annuli segments the WSB and ASB in three parts (sWSB, cWSB, nWSB, sASB, cASB, nASB). Also, the TAM are segmented in three blocks (sTAM, cTAM, nTAM) and the same applies to the WARS (sWARS, cWARS, nWARS). To the north, the EAFBP is terminated by a dextral (in the SX sector) or sinistral (in the DX sector) transcurrent release fault system made up of en-èchelon strike-slip faults shown in Fig. 4. The final rotation angle of the TAM around point DP is $\alpha \cong 20°$.
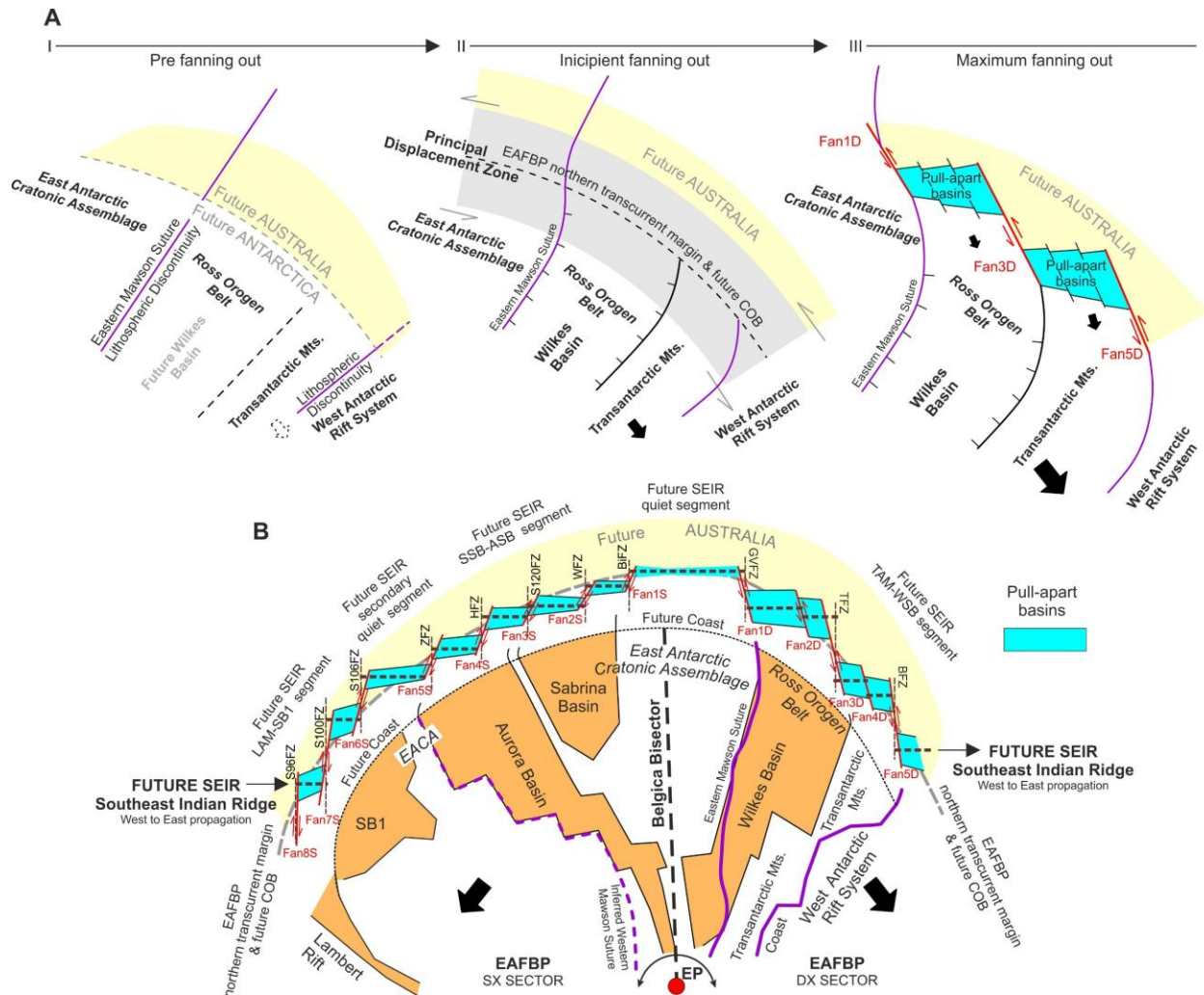
Figure 4. Northern EAFBP transcurrent fault release system evolution explaining the semi-circular asymmetric curvature of the Antarctic/Australian continent ocean boundary and coastlines and the observed present-day distribution of the oceanic fracture zones.

(A) Simplified sketch showing in detail the proposed model for the early-stage evolution of the northern EAFBP transcurrent fault release system along the dextral EAFBP sector; in the sinistral sector a specular evolution is expected. I) Before the fanning out, the presence of pre-existing lithospheric discontinuities is assumed (the Eastern Mawson Suture at the edge of the EACA and the TAM-WARS discontinuities). II) During the incipient fanning out, pre-existing lithospheric discontinuities and/or newly forming longitudinal EAFBP normal faults are left laterally deformed along the sinistral principal displacement zone that accommodates the EAFBP rotational extension against the fixed future continental Australia. III) With increasing rotational extension, a set of overlapping en-èchelon left-lateral strike-slip faults (red lines: Fan1D, Fan3D, Fan5D) develop in the principal displacement zone along the lines of weakness originated by the bended pre-existing lithospheric discontinuities and the newly formed EAFBP longitudinal normal faults. Secondary

strike-slip faults (not shown) are also expected to form. Pull-apart basins (cyan color in the figure) will develop between overlapping strike-slip faults, likely formed by many smaller coalescent pull-aparts and eventually will evolve into short seafloor spreading segments. Note that the pull-aparts are expected to be asymmetric since the offsets of the strike-slip faults increase towards the outside of the fan.

(B) Simplified sketch of the strike-slip fault system (red lines) that compose the whole northern EAFBP transcurrent fault release system in the final stage. The lateral offset along the faults increases towards east and west from the BB central arm of the fan. The overlapping strike-slip faults originate approximately east-west pull-apart basins that will drive the SEIR propagation (dashed thick brown lines), the correspondent orthogonal fracture zones (dashed thin brown lines) and consequently the location and shape of the future continent ocean boundary (COB, thick gray line) and coastline (thick black dashed line) at the conjugated Antarctic and Australian margins (see also Fig. 2). In the brittle crust, extension is expected to be accommodated at discrete steps by the sketched strike-slip fault system (red lines). At the central sector of the fan, around the BB bisector, strike-slip fault offsets are very low. At the dextral sector, the location of the strike-slip faults is controlled by lithospheric discontinuities marking the EACA-WSB, WSB-TAM and TAM-WARS limits. The offset along them is favored by the weakness due to the pre-existing discontinuities and to the thinner ROB lithosphere and is therefore higher than on the sinistral sector at the same distance from the Belgica bisector, generating an increase of the curvature of the future COB and higher extensional strain e_{DX} in the dextral sector ($e_{DX} > e_{SX}$). Some remnants of the fault system are expected along the present-day (see Fig. 2) passive margin in the dextral (eastern) EAFBP sector as sinistral strike-slip faults clockwise rotated relative to the margin, with possible associated subsidiary shear faults, transtensional/transpressional basins along each fault and pull-apart basins in the overlapping regions between the faults. Similar structures with specular orientation are expected in the sinistral (western) EAFBP sector.

EXTENDED DATA

| Acronym	Name	Shape	Annulus	Sector	Bisector	References
WSB	Wilkes Basin	V-shaped	s, c, n	DX		74
ASB	Aurora Basin	V-shaped	s, c, n	SX		74
ST1			c	DX		
ST2			c	DX		
ST3		V-shaped	c, n	DX	yes	
ADV	Adventure Subglacial Trench	V-shaped	c	DX	yes	75
ST4		V-shaped	c, n	SX		
PEA	Peacock Subglacial Trench		c	SX		75
AUR	Aurora Subglacial Trench	V-shaped	c	SX		
VOS	Vostok Lake Subglacial Trench	V-shaped	c	SX	yes	
90E	90°E Lake Subglacial Trench		c	SX		76
sEEARS	Eastern East Antarctic Rift (southern segment)		s	SX		9
cEEARS	Eastern East Antarctic Rift (central segment)		c	SX	yes	9
nEEARS	Eastern East Antarctic Rift (northern sector)		n	SX		9
WEARS	Western East Antarctic Rift		s	SX		9
EAB	Eastern Basin		n	DX		26
CEB	Central Basin		n	DX		26
WEB	Western Basin - Webb Basin		n	DX		26
AST	Astrolabe Subglacial Basin		n	DX		76
FRO	Frost Subglacial Basin	V-shaped	n	DX	yes	77
ST5		V-shaped	n	DX	yes	
SAB	Sabrina Subglacial Basin	V-shaped	n	SX	yes	77
ST6			n	SX		
ST7			n	SX		
ST8			n	SX		
SHM	Shmidt Subglacial Basin		n	SX		25
KNO	Knox Subglacial Basin		n	SX		77
ST9			n	SX		
SB1		V-shaped	n	SX	yes	
LAM	Lambert Graben		n	SX		78

Extended Data Table 1.

List of the basins in the EAFBP, their acronyms and main characteristics. Shape: the term "V-saheped" is used to describe the pronounced convergence of the basin bounding faults toward a pivot point or pole. Annulus: southern sTAN (s), central cTAN (c) and northern nTAN (n) Transantarctic Annulus of the EAFBP where the basin is located. Sector: dextral (DX) or sinistral (SX) EAFBP sector where the basin is located. Bisector: for the basins marked by 'yes', the bisector of the triangular basin has been used rather than the two longitudinal edges in the

computation of the Euler Pole (Methods). SBn and STn acronyms (n integer number) are used for unnamed subglacial basins and trenches respectively.

| Evidence Acronym	Evidence description
T-EV01	The basins forming the EAFBP are elongated along the north-south direction and many show an approximately V-shape, forming a fan (see Extended Data Tab. 1 for a complete list)
T-EV02	The fan appears to have an axis of symmetry passing through the Belgica Subglacial Highlands (at ~130°E) that divide the EAFBP in the dextral (DX) and sinistral (SX) sectors.
T-EV03	Great circle fitting longitudinal basins' edges intersect around the mean location EP at 86.4° S, 129.9° E
T-EV04	WSB and ASB are dissected and offset along two circular belts (sTCSB and nTCSB) that may be interpolated by two small circles whose Euler pole locations (sEP: 84.2°S, 130.8°E; nEP: 83.1°S, 129.5°E) situated close to the Euler pole EP.
T-EV05	Along sTCSB and nTCSB belts, the WSB appears systematically offset by dextral shear, the ASB by sinistral shear.
T-EV06	The WSB and ASB mean bed elevation shows three relevant variations in relation to the sTCSB and nTCSB belts.
T-EV07	The coast limiting the EAFBP to the north has a semi-circular shape with increased curvature along the DX sector. On average, it may be interpolated from Cape Adare to Prydz bay by a small circle whose Euler point cEP is located at coordinates 81.7°S, 115.1°E, close to the estimated Euler poles EP, sEP, nEP
T-EV08	The sTCSB and nTCSB belts divide the EAFBP into three annuli sTAN, cTAN, nTAN
T-EV09	The nTAN is delimited to the north by the coastline and by the continental passive margin
T-EV10	The cTAN and nTAN contain many secondary basins and trenches, some inside the larger WSB and ASB and some outside, with V or rectangular shape
T-EV11	WSB and ASB show an increasing apparent eastern and western offset towards the north, suggesting an increase in the extensional shear along the three annuli
T-EV12	Between the Nimrod and Byrd glaciers the TAM show a deflection in their trend of ~20° with respect to their southernmost linear trend
T-EV13	The TAM are segmented and apparently right lateral offset along the sTCSB and nTCSB shear belts forming three main distinct blocks sTAM, cTAM, nTAM
T-EV14	The WARS grabens in the Ross Sea appear clockwise rotated
T-EV15	The WARS grabens in the Ross Sea appear lateral offset along two major lithospheric discontinuities that represent the continuation of the sTCSB and nTCSB into the Ross Sea
T-EV16	The EARS is segmented and left lateral offset along the sTCSB and nTCSB belts
T-EV17	Off-shore, fractures zones (FZ) along the Southeast Indian Ridge (SEIR) are more closely spaced and prominent in front of the TAM and WSB to the east and of the SB1, SSB and ASB to the west with respect to the sector facing the symmetry axis BB of the fan. On the base of FZ spatial density and ridge offsets, the SEIR is segmented in: i) the TAM-Wilkes segment, ii) a central 'quiet' segment, iii) the Sabrina-Aurora segment, iv) another secondary 'quiet' segment, v) the Lambert-SB1 segment
T-EV18	The curvature of the semi-circular Antarctic coast line and COB is greater in the EAFBP dextral sector compared to the sinistral one
G-EV01	A crustal depth model based on integrated seismic and gravimetric data[30] indicates thinned crust corresponding with the major basins in the EAFBP
G-EV02	The GSM are located on a thick crustal belt with lithospheric roots deeper than 200 km compatible with crustal/lithospheric horizontal shortening[79]
G-EV03	The Lake Vostok trough is formed by a major geological boundary[24,25] apparent in magnetic and Bouguer gravity anomalies
G-EV04	The western flank of the WSB features a sharp magnetic[26,27] and gravimetric[28] break that defines the boundary (Eastern Mawson Suture) between the thick and highly magnetic Mawson continent of the East Antarctic Cratonic Assemblage[29] (EACA) and the thinner and weakly magnetic Ross Orogen belt[19,23,27]
G-EV05	Two low velocity zones at upper mantle depth (~150 km) have been imaged by Rayleigh wave phase velocities models[46,47] beneath Ross Island and offshore Mt. Melbourne, along the sTCSB and nTCSB.

Extended Data Table 2.

Summary of the topographical and geophysical evidence that are explained by the proposed kinematic model. EAFBP: East Antarctic Fan-shaped Basin Province. GSM: Gamburtsev Subglacial Mts. TAM: Transantarctic Mts. sTCSB, nTCSB: southern and northern Transantarctic Circular strike-slip Shear Belts. WSB: Wilkes Subglacial Basin. ASB: Aurora Subglacal Basin.
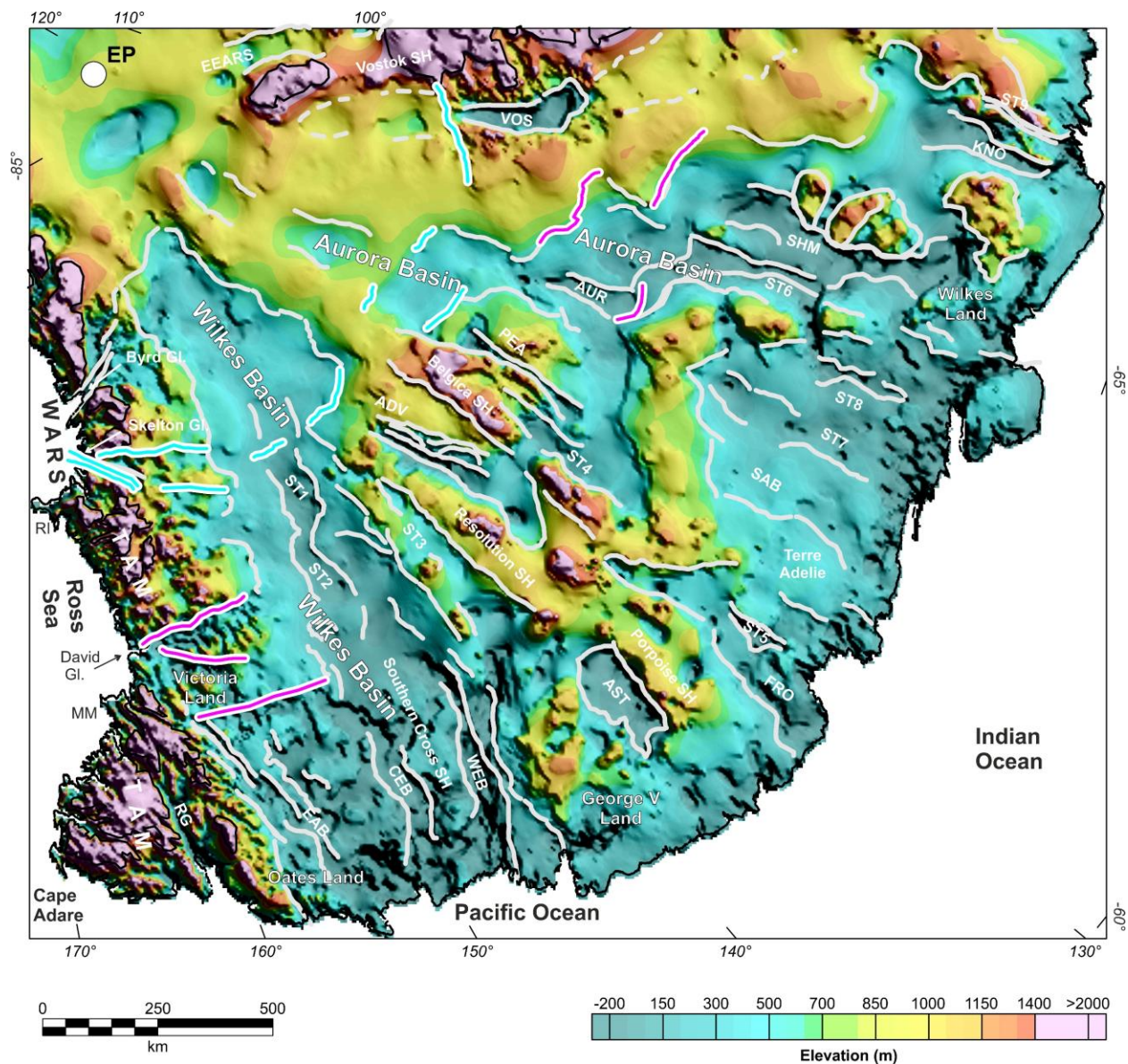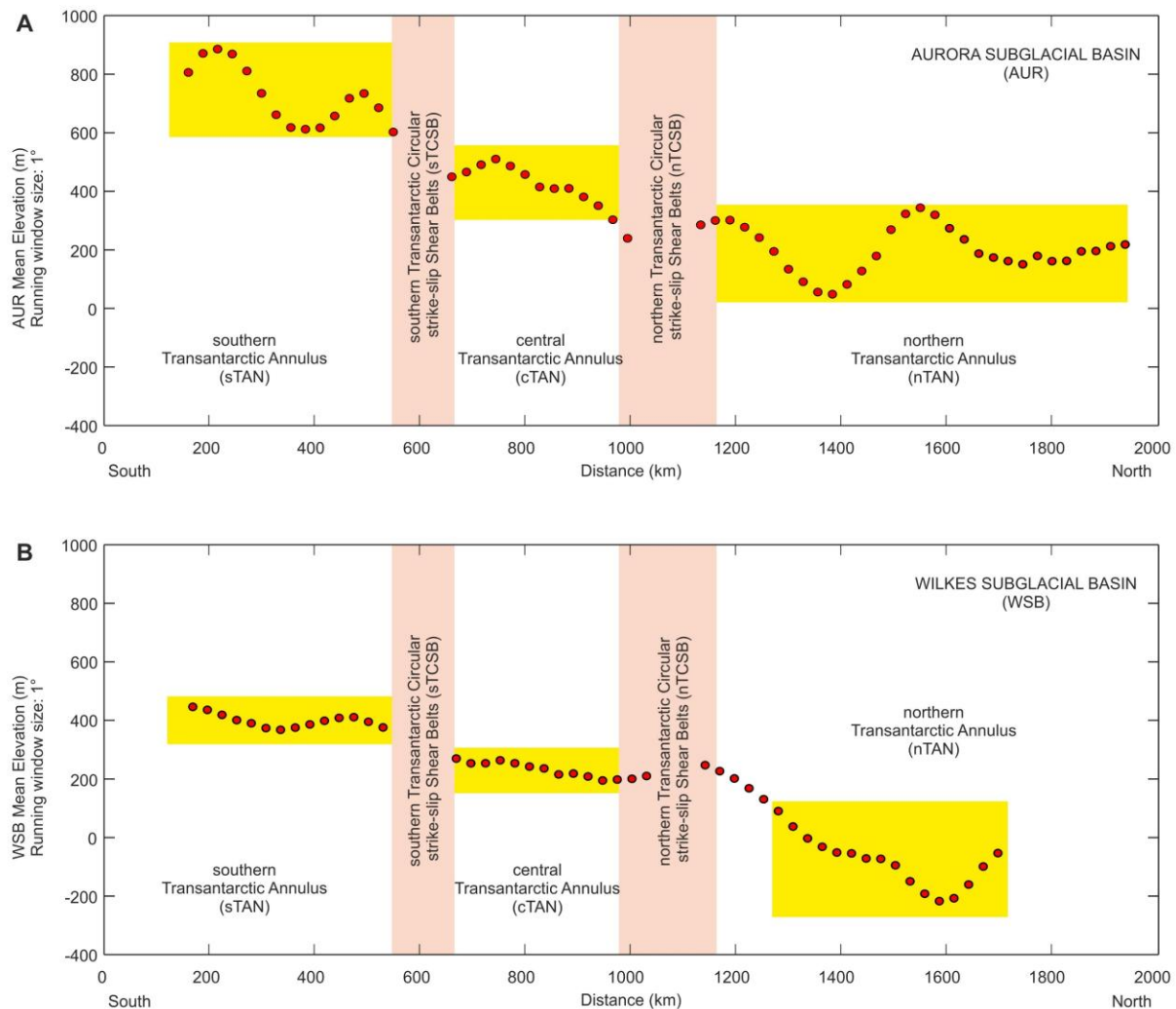
Extended Data Figure 1.

Detail of the fault system composing the EAFBP. Enlargement of the main sector of the EAFBP including the main triangular basins. Note the north-south normal faults (light gray lines) and circa east-west strike-slip faults with associated transtensional conjugate faults (cyan and magenta lines).
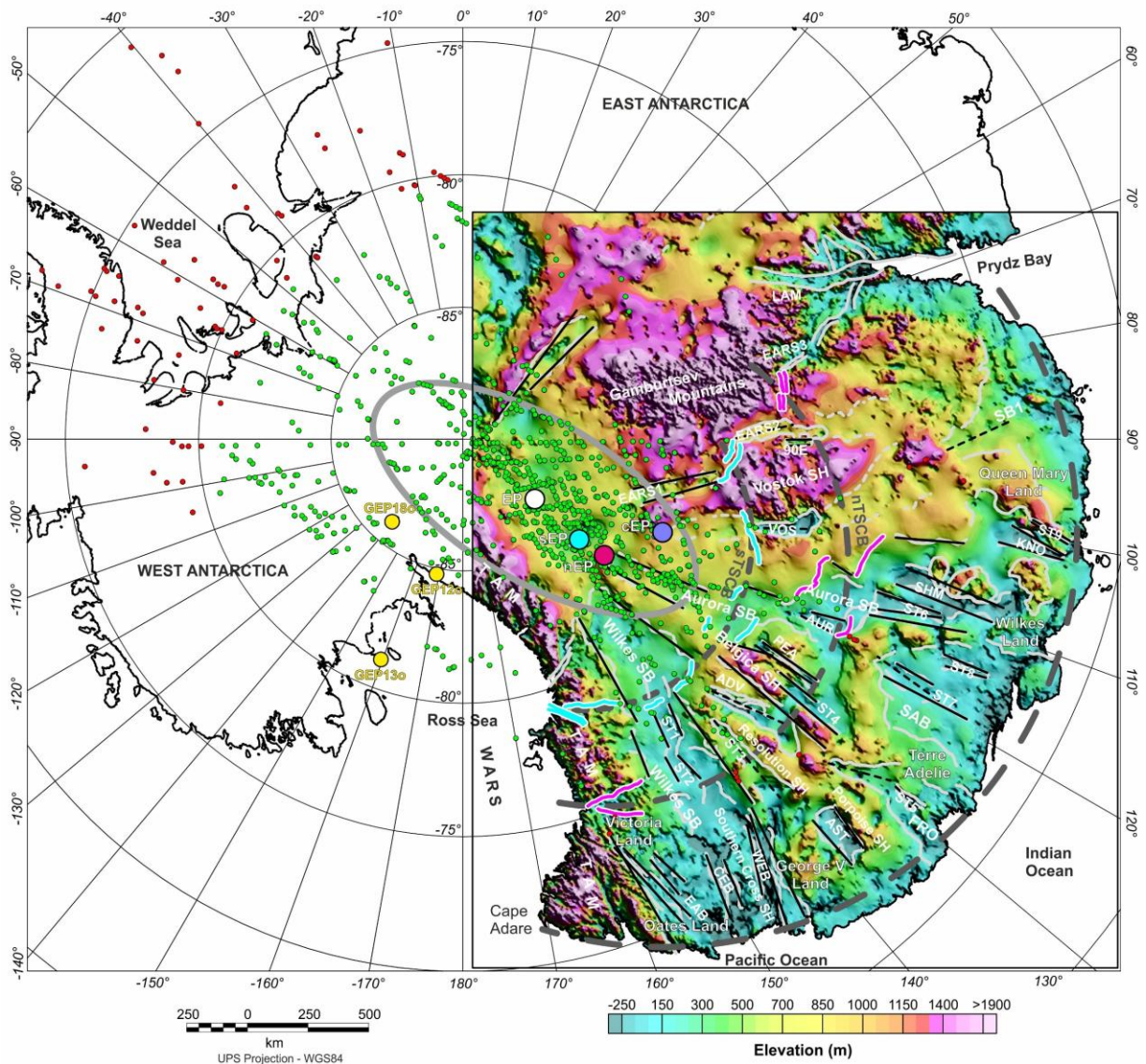
Extended Data Figure 2.

Estimation of the Euler Pole (EP) of the EAFBP. The detected topographic lineaments, traced by the semiautomatic methodology applied to the filtered rebounded topography (color map, Methods), are interpreted as circa north-south normal faults (light gray lines) and circa east-west strike-slip faults with associated transtensional conjugate faults (cyan and magenta lines). The longitudinal normal faults forming the structural edges of the basins (light gray lines) have been fitted by segments of great circles (black straight lines) and their intersections have been computed (red and green small circles). For some basins the bisector (dashed black lines) of the longitudinal edges has been considered in place of the converging edges (see Extended Data Tab. 1). The pivot point EP (large white circle) has been estimated as the mean location of the green intersection points (red intersection points have been discarded). The error ellipse (light gray line) is the

minimum area ellipse containing 68% of the green intersection points. The transversal east-west strike-slip faults or prevalent east-west normal faults associated to transtension (magenta lines) that identify the nTAN shear belt have been fitted by a small circle (dashed dark gray line) whose computed Euler Pole nEP is marked by a large magenta circle. The transversal strike-slip faults or prevalent east-west normal faults associated to transtension (cyan lines) that identify the sTAN shear belt have been fitted by a small circle (dashed dark gray line) whose Euler Pole sEP is marked by a large cyan circle. The coastline has been fitted by a small circle (dashed dark grey line) whose Euler Pole cEP is marked by a large violet circle. The locations of the three estimated additional Euler poles (sEP, nEP, cEP) are consistent within the EP error ellipse. GEP12o, GEP13o, GEP18o: best-fit rotation poles[51] for relative motion between East (fixed) and West Antarctica for magnetic subchrons 12o (30.9 Ma), 13o (33.5 Ma) and 18o (40.1 Ma) respectively.

Extended Data Figure 3.

Wilkes and Aurora basins bed mean elevation pattern.
Wilkes and Aurora basins bed mean elevation (red dots, rebounded topography) has been computed along circular running windows made by one-degree annuli centered at the mean location of poles sEP and nEP. The distance from the mean pole (in km) of the corresponding window is reported in the horizontal axis. The southern and northern Transantarctic Circular strike-slip Shear Belts (sTCSB and nTCSB, pink areas) divide the Wilkes and Aurora basins in three main zones corresponding to the southern, central and northern Transantarctic Annuli (sTAN, cTAN and nTAN). The mean bed elevation over the three annuli shows three different levels (yellow stripes) rather than a linear trend. Note that for the Wilkes a third topographic step may be present at about 1500 km, possibly marking the northern EAFP transform fault limit; however, this interpretation might be biased by the strong ice erosion at the coastline.
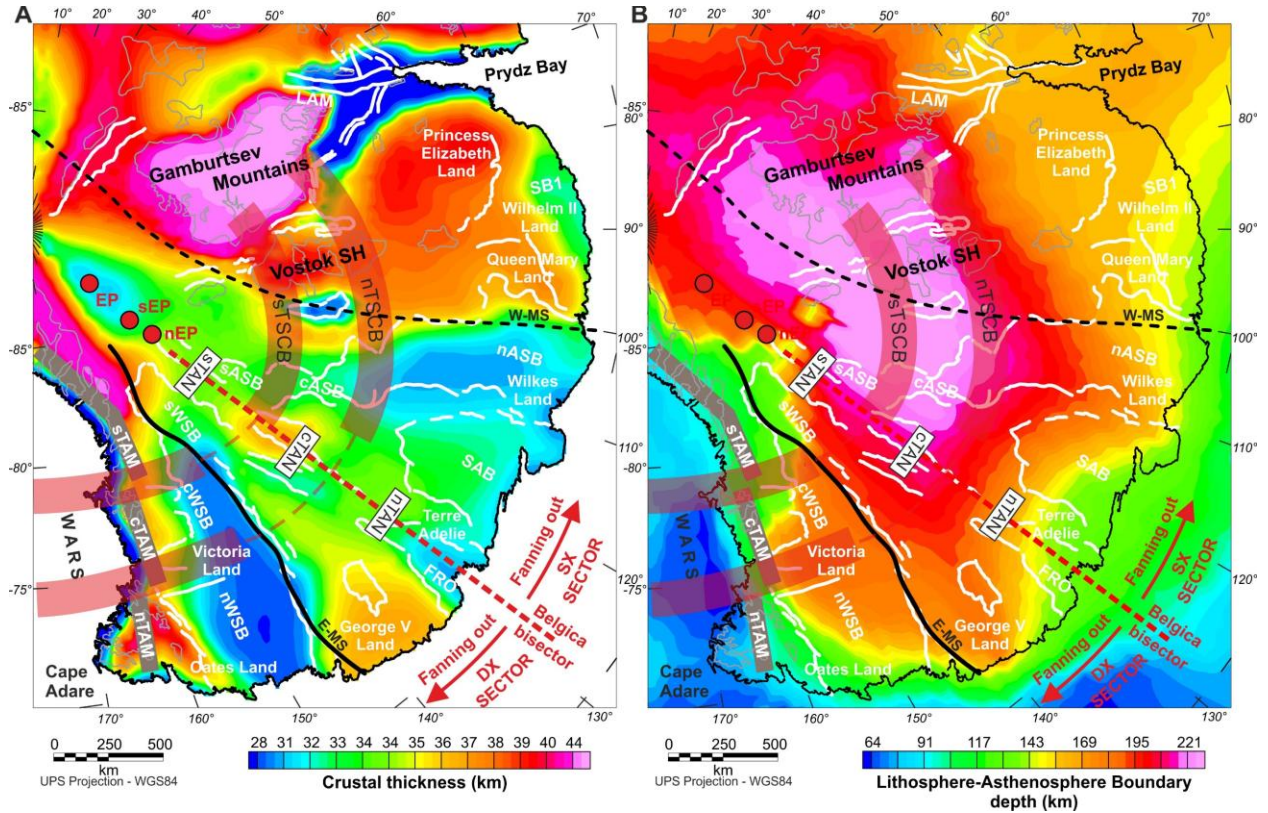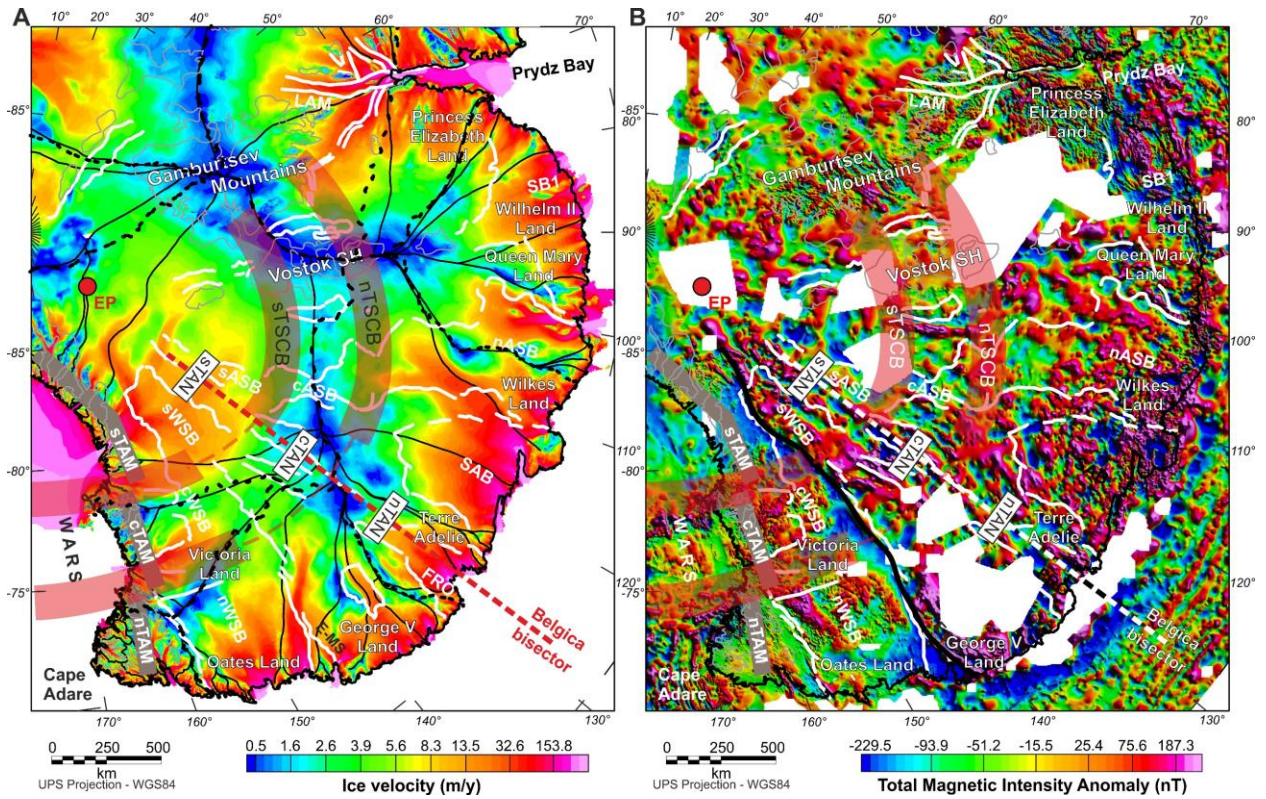
Extended Data Figure 4.

Location of the main structural features of the EAFBP compared with the estimated crustal thickness distribution and the shear-wave (SH) velocity perturbations in the lithosphere.

(A) Main structural features of the EAFBP superimposed on the crustal thickness map derived from joint analysis of gravity and seismic data[30]. We interpret the observed reduced crustal thickness in correspondence of the main EAFBP basins as indicative of the rotational extension. The proposed segmentation and offset of the TAM in the three blocks (sTAM, cTAM, nTAM) based on the topographical and geological evidence is confirmed in the crustal thickness map. E-MS: Eastern Mawson Suture. W-MS: Western Mawson Suture. EP: EAFBP pole. sEP, nEP: poles of the southern and northern Transantarctic Circular strike-slip Shear Belts. White heavy lines: main basins in the EAFBP.

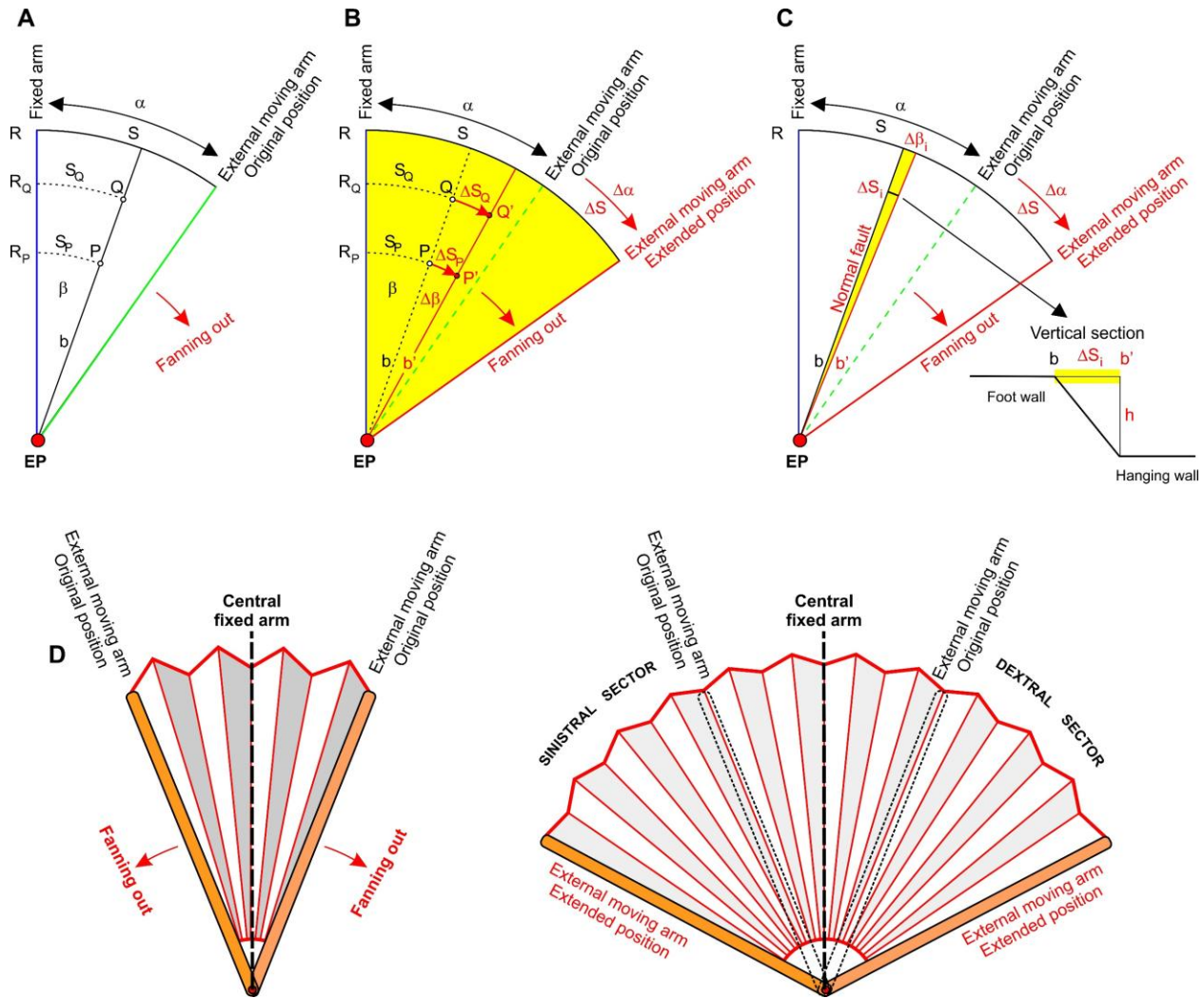(B) Main structural features of the EAFBP superimposed on the Lithosphere-Asthenosphere Boundary depth[31]..

Extended Data Figure 5

Ice velocity and magnetic maps over the EAFBP.

(A) Ice velocity map and and ice basins' divides[37].

(B) Total Magnetic Intensity map[27]

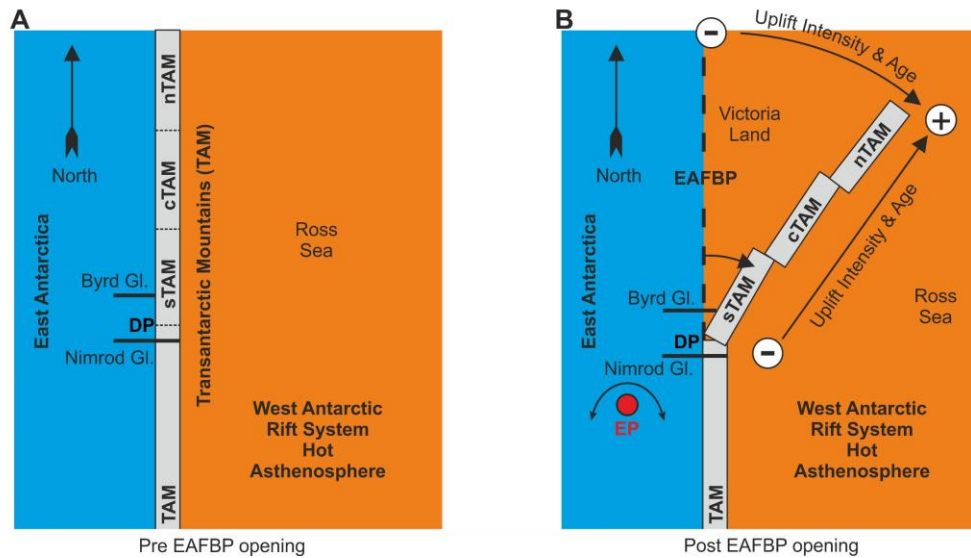**Extended Data Figure 6.**

Rotational extension kinematic

(A) Folded fan before extension. Only the right sector is shown for simplicity. The fan angle between the fixed arm and the external arm is α and the length along the external arc is S. P and Q are points along the same stick b of the fan at a distance (along the arc) SQ and SP and angular distance β from the fixed arm. RP and RQ are the distance from the pivot point EP.

(B) Folding out of the fan to the right, in the case of continuous deformation. The external moving arm is rotated clockwise by an angle $\Delta\alpha$ that corresponds to the length Δs along the arc. The ratio $e=\Delta\alpha/\alpha=R\Delta\alpha/R\alpha=\Delta S/S$ defines the extensional strain of the fan. The internal stick b is rotated in b' by an angle $\Delta\beta$ such that $e=\Delta\beta/\beta$. The two points P and Q are displaced in P' and Q', following a trajectory along the arcs of radii RP and RQ (rule R1). The displacements ΔS_P and ΔS_Q are such

that $e=\Delta S_P/S_P=\Delta S_Q/S_Q$ (rule R2). Note that, along the same stick, the displacement increases moving away from EP: $\Delta S_Q>\Delta S_P$ when $R_Q>R_P$ (rule R3).

(C) Folding out of the fan to the right, in the case of brittle deformation accommodated by a set of radial normal faults (only one is drawn) forming the longitudinal edges of the main basins. Each normal fault contributes to accommodate the total extension $\Delta\alpha$ by a small angle $\Delta\beta_i$. The increasing linear displacement ΔS_i moving away from EP implies an increasing vertical displacement h along the fault and a consequent increasing sinking of the hanging wall.

(D) Analogy between the rotational extension model and opening of a handheld fan
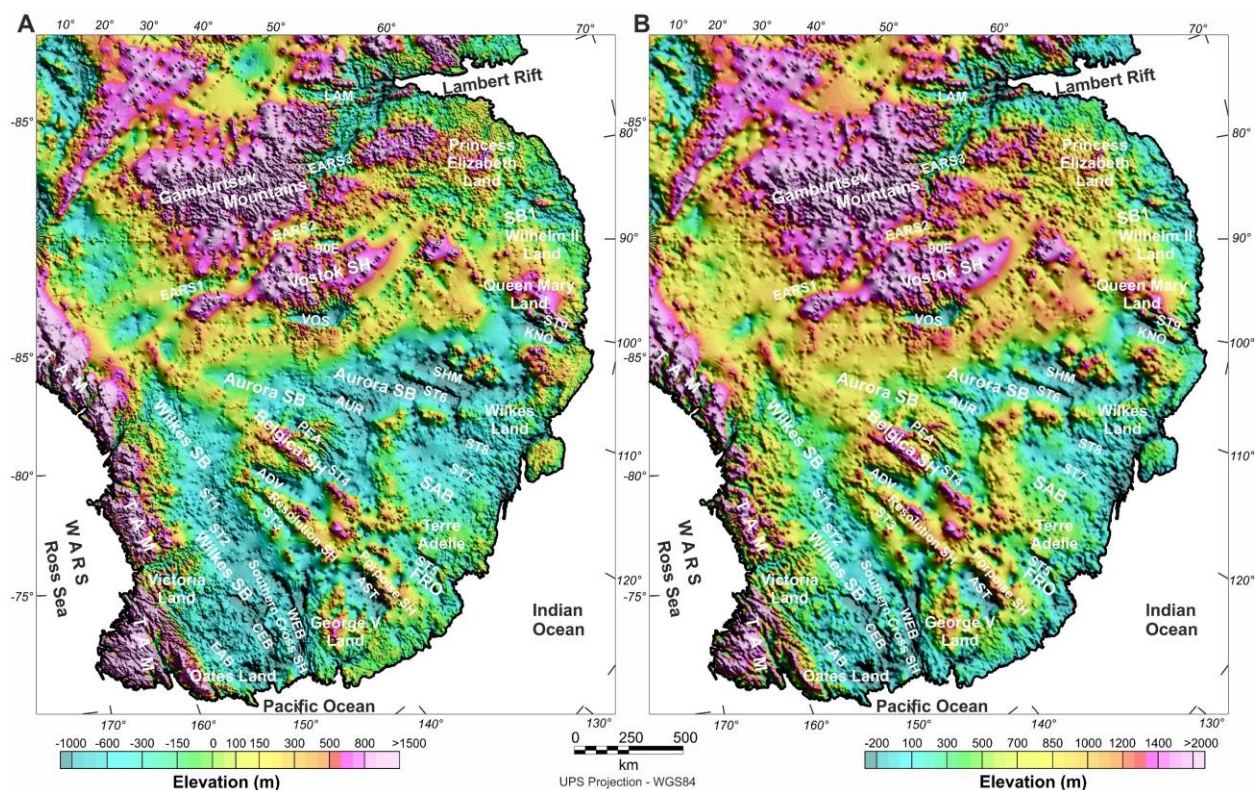
Extended Data Figure 7.

Expected intensity and age trend of the additional TAM uplift caused by their overriding over the hot West Antarctic lithosphere due to their clockwise rotation and segmentation.

(A) Pre EAFBP situation. NG: Nimrod Gl.; BG: Byrd Gl.

(B) Post EAFBP fanning out. The fanning out of the EAFBP pushed the sTAM, cTAM and nTAM blocks eastward, overriding the hot West Antarctic Rift System lithosphere. Due to the rotational extension, the northernmost nTAM sector was the first to significantly override the WARS lithosphere and reached the easternmost location, with consequent greater thermal buoyancy. Additional uplift intensity is therefore expected to be older and more intense towards the coastal sector of nTAM, decreasing inland, as hypothesized by some interpretations of apatite fission-track thermochronology[80]. At the same time, moving towards south along the coast, through the cTAM and sTAM blocks, the additional uplift intensity is expected to decrease and become younger.

Extended Data Fig. 8.

Sub ice topography before and after rebound.

(A) BedMachine[2] sub-ice topography.

(B) Adjusted topography for the isostatic effect of ice sheet removal[55], obtained computing the flexural response to the complete removal of the modern grounded ice load using an elastic plate model with a laterally variability flexural rigidity and accounting for the disequilibrium associated with the ongoing response to ice mass changes since the Last Glacial Maximum. The original grid has been down-sampled to 5000 m. Note the different color scales in the two maps.

METHODS

Sub-ice topography isostatic adjustment

For the Antarctic bed topography, we used version 3 of the BedMachine compilation[66]. BedMachine derives bed elevation and ice thickness using a combination of mass conservation in regions of fast ice flow along the periphery of the ice sheet and streamline diffusion to interpolate between radio-echo sounding line data in the slow-moving interior. The nominal resolution of the BedMachine grid is 500 m, but we down-sampled this to 5000 m to facilitate faster computation. We then adjusted the topography for the isostatic effect of completely removing the modern ice sheet load ([Extended Data Fig. 8](#)). For this, we used a pre-existing calculation[55], which computes the flexural response to the complete removal of the modern grounded ice load[2] using an elastic plate model with a laterally variability flexural rigidity, that also accounts for the disequilibrium associated with the ongoing response to ice mass changes since the Last Glacial Maximum. For simplicity, we referenced our rebounded topography to modern global mean sea level. We did not make any adjustments for post-34 Ma erosion, sedimentation, or associated isostatic adjustments, since correcting for these processes tends to smooth the topography, whereas the focus of this study is detecting changes in slope associated with tectonic structures.

Basin-edge detection

In order to trace the edges of the topographic subglacial basins within the EAFBP, we first applied a non-linear terracing filtering procedure to remove smooth, low-amplitude signals from the topography while preserving the sharper and higher-amplitude topographic variations. For an original topography, t0, and a filtered output topography, t, covering an area A, the procedure is based on an iterative algorithm that minimizes the Tikhonov parametric functional $T^{\alpha}(t)$, which is the weighted sum (by factor α) of two components:

$$T^{\alpha}(t) = \varphi(t) + \alpha \cdot S^{\beta}_{mgs}(t)$$

Where:

$\varphi(t)$ is a misfit functional determined as the norm of difference between true (t0) and output filtered (t) topography; it controls the closeness of the filtered output t to the original input topography t0:

$$\varphi(t) = \|t_0 - t\|$$

$S_{mgs}^{\beta}(t)$ is the minimum gradient support functional[66] defined as

$$S_{mgs}^{\beta}(t) = \int_A \frac{\nabla t \cdot \nabla t}{\nabla t \cdot \nabla t + \beta^2} dA$$

In this equation, the terms where the gradient ∇t is much less than β have zero contribution, while terms where any gradient much larger than β exists have contributions equal to one. Thus, sharp boundaries in topography are promoted and, consequently, enhancement of the edges of the basins, which are associated with steep topographic gradients, are obtained.

We then highlighted the strong variations in topography, that are expected to coincide with the flanks of the basins, by computing the magnitude of the horizontal gradient. The lineaments were then traced manually following the significative peaks. The process was assisted by automatic procedures such as the use of the phase congruency operator[68] to trace the local positive picks and the Hough transform to trace the correspondent lineaments[69]. The final set of basin edges (Fig. 1) is the result of this automatic procedure mixed with careful visual inspection and manual corrections. On the basis of the results, we identified 30 basins that are listed in Extended Data Tab. 1.

Estimation of the Euler poles

The Euler pole describing the rigid rotations that formed the EAFBP was estimated from the longitudinal edges of the basins that are expected to align along great circles that intersect at the Euler pole, which can also be visualized as the pivot point of the fan. First, we fitted the longitudinal edges of the basins to great circles in a least square sense and computed all the intersections between the extrapolations of these circles on a 3D Earth (Extended Data Fig. 2). For some of the basins with triangular shape (see Extended Data Tab. 1), we interpolated a great circle along the bisector instead of the longitudinal edges. We considered 60 great circles and obtained 1103 intersections (Extended Data Fig. 2), excluding those to the north of the EAFBP. Not all the intersections may be considered representative of the EAFBP Euler pole, since the direction of some of the basins' edges may have been strongly affected by inherited discontinuities or some of the basins may have not been formed in association with the EAFBP. Therefore, we applied an iterative scheme to remove outliers defined as the intersections that are more than three scaled median absolute deviations (MAD) far from the pole, obtaining the final 1025 intersections after 12 iterations. The Euler pole with coordinates 86.4°S, 129.9°E (WGS84) was estimated as the mean point of the final intersections. The ellipse error was computed as the area containing 68% of the intersections (resulting ellipse semiaxes: 750 and 330 km; azimuth of the major semiaxis at the EP: N8.9°W).

The two poles sEP (84.2°S, 130.8°E WGS84) and nEP (83.1°S, 129.5°E WGS84) for the southern and northern Transantarctic Circular strike-slip Shear Belts were estimated looking for the two small circles on the spherical Earth that are closer (in the least square sense) to the structural features defining the two belts shown in Extended Data Fig. 2. The pole cEP (81.7°S, 115.1°E WGS84) for the coast was estimated looking for the small circle on the spherical Earth that is closer (in the least square sense) to the coastline between Cape Adare and Prydz Bay (Fig. S2).

SUPPLEMENTARY INFORMATION

The rotational extension model

Dynamics of rotational extension near a Euler pole has been recently investigated by numerical and analog studies and many examples of triangular basins and rifts have been recognized all over the world[32-35,41,42,70,71]. Rotational extension (Extended Data Fig. 6) is expected to be continuous in the lower crust and brittle in the upper crust and is controlled by some simple rules. i) During the fanning out, each stick of the fan is rotated rigidly around the pivot point and, therefore, each point of the fan describes an arc of circumference. ii) The displacement of any point is proportional to its original distance, along the arc, from the fixed arm, where the constant of proportionality is the extensional strain of the fan. iii) For each point along the same fan stick, the displacement increases moving away from the Euler pole. iv) In the case of rotational extension accommodated by brittle deformation along normal faults, it is expected that the strike of these faults aligns with radii from the pivot point, representing the plane projection of great circles passing through the Euler pole. v) Consequently, the vertical slip accommodating the increasing horizontal extension along a single fault plane must increase with distance from the Euler pole. To avoid the progressive sinking of a single triangular basin in the fan moving far from the Euler pole, secondary basins must open in the outermost region of the fan. In fact, in order to ideally maintain a constant subsidence of the crust caused by extension, it is necessary to have a constant number of radial faults (and consequently of triangular basins) per unit area of the fan. The expected final result is likely a combination of these two effects. Progressive sinking of the main triangular basins moving away from the Euler pole and a simultaneous increase in the number of basins and corresponding normal faults. This effect is clearly observed within the EAFBP, where progressive sinking moving to north is observed in all the basins and, at the same time, the number of secondary basins increases moving from the central to the northern annulus, where they also appear inside wider basins as predicted by some analogue models[34].

The asymmetry in the circular curvature of the EAFBP northern limit (and consequently in the future coastal line and continent-ocean boundary) between the sinistral and dextral sectors may be explained by i) the different rheological properties, in the sinistral sector, of the older and thicker lithosphere of the East Antarctic Cratonic Assemblage (Extended Data Fig. 4b) that limited strike-

slip offsets with respect to the Ross Orogen Belt lithosphere and ii) the pre-existence, in the dextral sector, of the two major lithospheric discontinuities, i.e. the Transantarctic Mountains - West Antarctic Rift System boundary and the Eastern Mawson Suture; these first order discontinuities accommodated locally most of the left-lateral offset, allowing for a higher extensional strain that caused the higher curvature of the dextral sector.

Consequences of the EAFBP fanning out on older structures

Older structures are expected[41,42] to be deformed by the EAFBP fanning out in a complex manner that depends on their location and original orientation with respect to the location of the Euler pole and the fixed arm of the fan. The Western Mawson Suture and the Transantarctic Mountains are approximately previous linear features passing very close to the Euler pole and approximately parallel to the Belgica bisector fixed arm. Therefore, they are essentially affected by a rotation around a deflection point (Fig. 3). Due to the rotation, the Transantarctic Mountains override the hot West Antarctic Rift System lithosphere and underwent additional uplift caused by differential thermal buoyancy (Extended Data Fig. 7). The Eastern Mawson Suture is closer to the Belgica bisector fixed arm and is therefore less affected by the rotational extension. The late-stage strike-slip deformation along the southern and northern Transantarctic Circular strike-slip Shear Belts caused the nowadays observed segmentation of the Transantarctic Mountains. The southern Transantarctic Circular strike-slip Shear Belt offsets the Transantarctic Mountains north of the Skelton Glacier, in correspondence with the Discovery accommodation zone[58]. The northern Transantarctic Circular strike-slip Shear Belt offsets the Transantarctic Mountains in the area between David and Tucker glaciers and coincides with other two previously observed lithospheric discontinuitiess[22].

Generally, reactivation of older structures accommodating the rotational extension[41,42] and large transtensional deformation induced by the differential fanning out are expected over the whole EAFBP. Pre-existing discontinuities along Byrd and Nimrod glaciers were likely reactivated, accommodating Transantarctic Mountains deflection. The observed diffuse Cenozoic right-lateral strike-slip reactivations of older north-west/east-west faults, marking the main glaciers intersecting the Transantarctic Mountains[72] and grabens like the Rennick Graben[73] in Victoria Land and in the Ross Sea, may have been generated by the opening of the EAFBP dextral (eastern) sector. In the

sinistral (western) sector, specular left-lateral strike-slip reactivations of possible older north-east/east-west trending structures are expected, as observed for instance in the Lambert Rift[11].

Lines of evidence consistent with strike-slip displacement at the northern edge of the EAFBP

The rotational extension model necessarily implies the development of strike-slip movements along the northern edge of the fan during its outward propagation. These were accommodated along sets of faults trending NW in the dextral sector and NE in the sinistral sector of the fan (red lines in Figs. 2 and 4), i.e. oblique to the overall N-S radial trend of the fan. This proposed en-échelon fault system is inferred to have generated a series of approximately E-W trending pull-apart basins that subsequently localized the rifting leading to the separation of Antarctica from Australia. The strike-slip faults, arranged en-échelon, defined the position of the main fracture zones in the oceanic crust, corresponding to the original offsets of the pull-apart basins (Fig. 4b). Direct remnants of these basins are not expected, as they would have been entirely obliterated by the younger rifting phase. However, evidence of the oblique strike-slip faults should be preserved close to the present-day Continent–Ocean Boundary (COB), on both the East Antarctic and Australian passive margins, facing the major oceanic fracture zones (Fig. 2b). Since these margins have been reworked by subsequent N-S rifting, buried beneath younger sediments and/or heavily modified by erosion, only limited traces of the proposed mechanism are likely to remain; additionally, it should also be emphasized that the Antarctic passive margin, where the EAFBP developed, is still very poorly explored. While future detailed investigations may further clarify these aspects, the following list summarizes the key lines of evidence supporting the model:

1) Semicircular Arc Geometry of the Continent-Ocean Boundary

The northern boundary of the EAFBP, coinciding with the Continent-Ocean Boundary, exhibits a pronounced arc-shaped geometry. This distinctive feature is accounted for by the proposed model, which predicts the formation of pull-apart basins aligned along the arc and necessarily controlled by the en-echelon strike-slip faults.

2) Correlation between main fracture zones and onshore main basin boundaries

According to our model, the en-échelon strike-slip faults derived from the bending of the onshore basin boundaries in the EAFBP and provided first-order structural templates that controlled the nucleation and propagation of the main oceanic fracture zones during subsequent seafloor spreading (Fig. 4b). The close correspondence between these oceanic fracture zones and the onshore basin boundaries in the EAFBP can be regarded as a remnant of this process and is clearly recognizable in Figs. 2a and 2b.

3) Magnetic and gravity signature of the Eastern Mawson Suture

On the Antarctic side, the prominent N-S trending magnetic and gravity lineament, interpreted as the signature of the Eastern Mawson Suture in the dextral sector of the EAFBP (Figs. 1 and 2),

shows a clear deviation toward the northwest approaching the COB, consistent with the model predictions for the main lineaments of the EAFBP dextral sector (Fig. 4a).

4) Prominent canyons on the continental slope oriented obliquely to the maximum slope

The continental slope exhibits several prominent canyons that cut obliquely across the direction of maximum slope (examples shown in Fig. 2, heavy red lines). These canyons most likely exploit pre-existing zones of crustal weakness, which may represent the preserved traces of the hypothesized en-échelon fault system, in line with the predictions of the proposed model.

Lines of evidence consistent with strike-slip displacement along the northern and southern Transantarctic Circular belts

Major strike-slip movements within the EAFBP predicted by our model are expected close to the point of deflection of the Transantarctic Mts. (e.g., Byrd and Beardmore glaciers), along the southern Transantarctic Circular strike-slip Shear Belt (e.g., Skelton Glacier) and along the northern Transantarctic Circular strike-slip Shear Belt (e.g., David, Priestley and Tucker glaciers). Unfortunately, even in the coastal areas along the Transantarctic Mts. the regional faults are hidden by the main glaciers, which make direct observations difficult. In fact, such direct geological/structural observations are very limited in number, sometimes ambiguous and, above all, difficult to date. In the following, we list the evidences that support the movements along the observed offset of the structural lineaments, upon which our model is based.

1) Distribution of Ferrar volcanics outcrops

The distribution pattern of Ferrar volcanics outcrops along the Ross Sea coast (Fig. 1b) strongly supports the hypothesis of the rotation of Transantarctic Mountains blocks together with dextral displacement. The Ferrar Supergroup is related to Middle Jurassic Gondwana-wide magmatic activity due to a large-scale extensional rift system[81]. Ferrar rocks (Kirkpatrick Basalt and Ferrar Dolerite) outcrop along the Transantarctic Mountains intruded into the Beacon Supergroup rocks of Devonian to Jurassic age and have been dated to around 176 Ma. Since they are older than the Transantarctic Mountains rotation and segmentation predicted by our model, they represent a good marker of any following displacement in this area.

The Jurassic Ferrar Supergroup distribution[57] is shown in Fig. 1b (Ferrar outcrops in orange). The Ferrar outcrops distribution is clearly rotated and offset in three blocks, strongly supporting the claimed rotation and the dextral strike-slip movement along the proposed southern and northern transantarctic circular strike-slip shear belts at their intersections with the Transantarctic Mountains. In our view, this is the strongest and clearest evidence supporting dextral movements and rotation within the dextral sector of the EAFBP.

2) Structural observations along the Priestley fault

Right-lateral strike-slip movements along the NW-SE trending Priestley fault has been observed from ground structural measurements[82]. The amount and age of the movement have not been directly measured. The Priestley fault is located along the northern Transantarctic Circular strike-

slip Shear Belt. Our model correctly predicts dextral strike slip movement along the shear belt in this area.

3) 1 km vertical offset of the Kukri erosion surface across the Byrd Glacier

The difference in elevation of the Kukri erosion surface across Byrd Glacier shows an apparent vertical offset of ca 1 km with south side up[83]. Assuming that horizontal movement caused the apparent vertical shift of the planar erosion surface this implies a dextral horizontal offset of ca 32 km, given the inclination of 1.8° towards west of the erosion plane surface. This observation is in accordance with our model which correctly predicts dextral movements in proximity to the Transantarctic Mts. deflection point (DP in Fig. 1).

4) Ross Sea observations

Major structural and physiographic features imaged in the Ross Sea exhibit large horizontal dextral offsets aligned along three subparallel zones (labelled CoopA, CoopB, and CoopC in Fig. 1b), which were interpreted as major transverse strike slip (East-West) basement faults[22]. These observations are in agreement with our model which predicts right-lateral dislocations in the Ross Sea. In essence, basement fault CoopC corresponds to the discontinuity predicted by the model near the rotation point of the Transantarctic Mts (DP in Fig. 1), CoopA and CoopB instead correspond to the dislocations predicted along the northern Transantarctic Circular strike-slip Shear Belt.

5) Regional right lateral strike-slip Cenozoic movements in northern Victoria Land

Right lateral strike-slip tectonic in northern Victoria Land has been widely documented from structural observations in the published literature along major NW-SE trending Paleo/Mesozoic(?) reactivated trending faults[72] interpreted as Cenozoic reactivation[82,84,85]. However, given the uncertainties in dating, older similar movements might have been the consequence of the EAFBP rotational extension. In fact, right lateral strike-slip shift is coherent with dextral shift along the Transantarctic Circular strike-slip Shear Belts.

6) Inferred sinistral lateral strike-slip movements in the Aurora Basin area

In the Aurora Basin area (sinistral sector of the EAFBP), an intraplate transtensional corridor has been proposed[86] with a left-lateral movement component, on the grounds of geological/structural observations and numerical models. Such tectonic scheme is compatible with the expected sinistral offset along both Transantarctic Circular strike-slip Shear Belts in the sinistral sector of EAFBP.

7) Statistical significance of distribution of direction of transverse offsets

Trasversal offsets are not randomly distributed. First, they are particularly evident along the two semi-circular bands that are approximatively centered on the proposed rotation pole of the fan, indicating a clear relationship among them. Secondly, the radial structural pattern is systematically offset to the right in the dextral EAFBP sector and to the left in the sinistral sector. This systematic relationship between the sense of offset and its spatial position is unlikely to be coincidental. The proposed model offers the required explanation to account for such spatial consistency in the observed offsets.

8) Inferred trasversal faults along the Transantarctic Mts.

Many approximatively EW oriented faults that have been inferred to underlie the major TAM outlet glaciers[20]. They are hypothesized to have accommodated differential movements between major structural blocks on the TAM frontal fault system, and also be locally reactivated from Neoproterozoic transfer faults. These faults may have been reactivated as strike slip faults to accommodate the rotational tectonics predicted by our model.

9) Distribution of the secondary basins within the EAFBP

Whereas the two major Wilkes and Aurora basins transect all three Transantarctic Annuli, the smaller basins are confined within the central and northern annuli. This distribution indicates a differentiation in extensional kinematics over the three annuli, which is consistently explained by the proposed rotational extension model.

10) Crustal thickness

The crustal thickness map[30] shown in Fig. 4a reveals a clear segmentation and dextral offset of the Transantarctic Mountains, bounded by the southern and northern Transantarctic Circular strike-slip shear belts, in agreement with the predictions of the proposed model.

Significance and Implications for East Antarctic Ice Sheet Dynamics

The proposed tectonic scenario, through its role in shaping the present-day East Antarctic landscape, carries three major implications for the behaviour of the East Antarctic Ice Sheet (EAIS).

First, there is strong evidence that the deep troughs generated by large-scale rotational extension exert a dominant control on basal hydrology and ice flow. This influence is manifested in two main ways: (i) by providing long-term storage for large volumes of water in vast subglacial lakes occupying the troughs, such as Lake Vostok[87], and (ii) by enabling the periodic evacuation of subglacial lake water toward the margin, as documented in the Adventure Subglacial Trench where a major subglacial flood and subsequent downstream discharge have been measured[88]. Such features and processes would not exist in the same way without the imprint of deep geological structures. Moreover, the association between deep troughs and ice surface slopes can make water flow-paths highly sensitive to even subtle changes in ice thickness, allowing minor upstream adjustments to lubricate the beds of entirely different ice sheet sectors**Error! Reference source not found.**.

Second, water may have begun to accumulate within these troughs soon after their formation (as proposed for Lake Vostok), offering the potential preservation of an ancient sedimentary archive of subaerial and later subglacial lacustrine environments[89]. Such records may uniquely capture the onset and subsequent evolution of Antarctic glaciation.

Third, the divergent geometry of the Wilkes and Aurora basins results in ice margins at the coast that are more than 500 km wide, with large portions grounded hundreds of metres below sea level.

This configuration makes extensive sectors of the EAIS margin particularly susceptible to rapid and irreversible retreat through marine ice-sheet instability processes[90] in a warming climate.

Taken together, these points highlight that, without the large-scale rotational extension that sculpted the sub-ice landscape, the evolution, behaviour, and climate sensitivity of the EAIS would likely have been fundamentally different.